

Colloidal Co single-atom catalyst: a facile synthesis strategy and high catalytic activity for hydrogen generation

Junkai Wang^{1, 2}, Zhenxia Huang^{1, 2}, Lilin Lu¹, Quanli Jia³, Liang Huang^{1}, Shuai Chang¹, Mingyang Zhang¹, Zuotai Zhang^{4*}, Sun Li⁴, Dongsheng He⁵, Wenhao Wu¹, Shaowei Zhang⁶, Naoki Toshima⁷, Haijun Zhang^{1*}*

1 The State Key Laboratory of Refractories and Metallurgy, Wuhan University of Science and Technology, Wuhan 430081, Hubei, P.R. China

2 School of Materials Science and Engineering, Henan Polytechnic University, Jiaozuo 454000, Henan, P.R. China

3 Henan Key Laboratory of High Temperature Functional Ceramics, Zhengzhou University, 75Daxue Road, Zhengzhou 450052, China

4 School of Environmental Science and Engineering, Southern University of Science and Technology, 1088 Xueyuan Road, Shenzhen 518055, P.R. China

5 Materials Characterization and Preparation Center, Southern University of Science and Technology, 1088 Xueyuan Road, Shenzhen 518055, P.R. China

6 College of Engineering, Mathematics and Physical Sciences, University of Exeter, Exeter Ex4 4QF, U.K.

7 Department of Applied Chemistry, Sanyo-Onoda City University (former Tokyo University of Science Yamaguchi), SanyoOnoda, Yamaguchi 756-0884, Japan

*Corresponding authors: Prof. Dr. Haijun Zhang, E-mail: zhanghaijun@wust.edu.cn

Dr. Liang Huang, E-mail: huangliang1986@wust.edu.cn

Prof. Dr. Zuotai Zhang, E-mail: zhangzt@sustc.edu.cn

Chemicals and materials

Potassium borohydride (KBH_4), cobalt nitrate hexahydrate ($\text{Co}(\text{NO}_3)_2 \cdot 6\text{H}_2\text{O}$), nickel nitrate hexahydrate ($\text{Ni}(\text{NO}_3)_2 \cdot 6\text{H}_2\text{O}$), iron nitrate nonahydrate ($\text{Fe}(\text{NO}_3)_3 \cdot 6\text{H}_2\text{O}$), sodium hydroxide (NaOH), poly(*N*-vinyl-2-pyrrolidone) (PVP), starch, carboxymethylcellulose sodium (CMC-Na), polyvinyl alcohol (PVA), sodium polyacrylate (PAAS) and polyethylene glycol (PEG) were purchased from Sinopharm Chemical Reagent Co., Ltd., China. Rhodiumchloride (RhCl_3), chloroplatinic acid ($\text{H}_2\text{PtCl}_6 \cdot 6\text{H}_2\text{O}$) and palladiumchloride (PdCl_2) were purchased from Aladdin. ISOBAM-104 (CAS.NO. 52032-17-4, average molecular weight of 55000~65000, see Figure S1 for its chemical structure) was purchased from KURARAY company, Japan. It is an amide-ammonium salt type of ISOBAM which is the trade name of a copolymer of isobutylene and maleicanhydride developed by KURARAY. All these raw materials were used directly without further purification. All glasswares and Teflon-coated magnetic stirring bars were cleaned with aqua regia, followed by copious rinsing with purified water. The water was purified by a PINGGUAN ultrapure water purification system (Wuhan, China). The hydrolysis tests of borohydride were carried out in an in-house designed device via measuring the mass of water displaced by the generated gas.

Instrumentation

Phases in samples were identified by powder X-ray diffraction (XRD) analysis using a Philips X'Pert PRO diffractometer (PANalytical, NETHERLANDS). Spectra were recorded at 40 mA and 40 kV, using Cu $K\alpha$ radiation ($\lambda=0.1542$ nm) between 30° and 80° (2θ). UV-Vis absorption spectra were recorded at 200-800 nm by a Shimadzu UV-2550 spectrophotometer (Shimadzu company, Kobe, Japan). Transmission electron microscopy (TEM) was performed on a JEM-2100F (JEOL company, Tokyo, Japan) Field Emission High-resolution transmission electron microscope with an electron acceleration energy of 200 kV. The specimens were prepared by dropping 2-3 droplets of the prepared colloidal aqueous solution onto a copper micro grid covered with a thin amorphous carbon film, followed by atmosphere drying at an ambient temperature. To evaluate the mean diameter, at least 200 particles from different locations on the grid were examined for each sample. Fourier transform infrared (FTIR) spectra of samples (embedded in KBr pellet) were recorded within the frequency range of $4000\text{--}400$ cm^{-1} and with a resolution of 4 cm^{-1} using an FTIR spectrometer (VERTEX 70, Germany). X-ray photoelectron

spectroscopy (XPS) was carried out on a VGMultilab 2000 instrument (Thermo Electron Co., USA) using 300 W Al K α as the excitation source. Samples in this case were subjected to high vacuum before being introduced into the analysis chamber. The binding energies from XPS were referenced to the C 1s binding energy (284.6eV) of “adventitious” carbon contamination. The high-angle annular dark-field scanning transmission electron microscopy (HAADF-STEM) was conducted on an FEI Titan Cubed Themis G2 300 with a spherical aberration corrector. Surface topography images of Co catalysts were taken using scanning probe microscopy (SPM, Keysight SPM 6500).

Preparation of ISOBAM-104 stabilized Co catalysts and catalytic hydrolysis of borohydride

The procedure used to prepare homogeneous ISOBAM-104 stabilized Co²⁺ colloidal catalysts was described as follows: a certain amount of ISOBAM-104 was added into a double-necked flask first, and then cobalt nitrate hexahydrate (Co(NO₃)₂·6H₂O) precursor. 50 mL of the mixed solution were stirred for 24 hours to obtain the desired catalysts.

The hydrolysis tests were carried out in a 250-mL round bottom flask equipped with a constant pressure drop funnel and placed in a thermostatic bath. Catalytic hydrolysis reaction of borohydride for hydrogen generation was initiated by dropping the fresh aqueous solution of potassium borohydride from the drop funnel to the flask and stirring the mixed solution of KBH₄ (10mL), Co(NO₃)₂·6H₂O and ISOBAM-104 (50mL). The mass of the water replaced by the released hydrogen was measured by using an electronic balance and was automatically recorded at intervals of two seconds. Before entering the water-ejecting instrument, the generated gas was allowed to pass through a trap containing concentrated sulfuric acid to remove any possibly produced ammonia. The long-time activity (catalytic durability) of the ISOBAM-104 stabilized Co²⁺ solution was examined by repeating the batch tests, in which case the following batch test was started by adding the same amount of solid KBH₄ into the ISOBAM-104 stabilized Co²⁺ solution upon the completion of the previous one.

It should be noted that the ISOBAM-104 used in this work contains NH₄⁺ group, which could act as a catalyst for hydrogen generation from hydrolysis of borohydride based on our previous work ¹. Therefore, to obtain the intrinsic catalytic activity of Co nanoparticles, the catalytic activities of ISOBAM-104 stabilized Co²⁺ and ISOBAM-104 (NH₄⁺ group) were respectively measured under the identical condition, and then

the catalytic activity value of ISOBAM-104 was subtracted from that of the ISOBAM-104 stabilized Co^{2+} .

In general, the hydrolysis experiment was carried out at ambient temperature (30 °C). The test conditions were varied to determine the kinetic parameters. All catalytic hydrolysis reactions were allowed to proceed for ~10 minutes and repeated at least three times under the identical conditions, and the mean values of the measured data were used to evaluate the catalytic activities. First, the optimum reaction conditions were determined by using a series of ISOBAM-104 solutions ($R_{\text{ISO}} = 10, 20, 30, 40, 50, 60$, R_{ISO} is defined as the molar ratio of ISOBAM-104 in monomer units to the total metal ions) and $\text{Co}(\text{NO}_3)_2 \cdot 6\text{H}_2\text{O}$ solutions (0.30, 0.45, 0.60, 0.75, 0.90, 1.20, 1.50, 1.80 mmol/L). Second, the apparent activation energy of hydrolysis of borohydride catalyzed by ISOBAM-104 stabilized Co^{2+} colloidal catalysts was evaluated based on several test runs at 20~40 °C. Third, the effects of different protective agents on the catalytic performance of Co^{2+} solution in the hydrolysis of borohydride were examined and compared. Finally, the catalytic activities of ISOBAM-104 protected noble metal NPs (Pd, Pt and Rh NPs) were also studied and compared with those of the ISOBAM-104 protected Co NPs.

The hydrogen generation rate (HGR, $\text{mL-H}_2 \cdot \text{s}^{-1}$) was determined in terms of the slope of the hydrogen volume-time plot during the initial reaction stage. The experimental data in the first minute were used for the kinetic analysis (such as apparent activation energy). The catalytic activities ($\text{mL-H}_2 \cdot \text{min}^{-1} \cdot \text{g-cat.}^{-1}$) were calculated in terms of the ratio of the hydrogen production rate to the catalyst. The intrinsic catalytic activity of Co NPs was calculated by subtracting the catalytic activity value of ISOBAM-104 from that of ISOBAM-104 stabilized colloidal Co^{2+} catalysts.

Quantum Chemical Calculations

DFT calculations were carried out using spin-polarization DFT/GGA with the PBE exchange-correlation functional, as implemented in the DMol³ package (BIOVIA company, San Diego, CA, USA). Double numerical basis set and polarization functions were carried out to describe the valence electrons, and an electron relativistic core treatment was used to perform full optimization of the investigated models without symmetry constraint. The convergence criteria were set to medium quality with a tolerance for self-consistent field (SCF), optimization energy, maximum force, and maximum displacement of 1×10^{-5} Ha, 2×10^{-5} Ha, 0.004

Ha/Å and 0.005 Å, respectively.

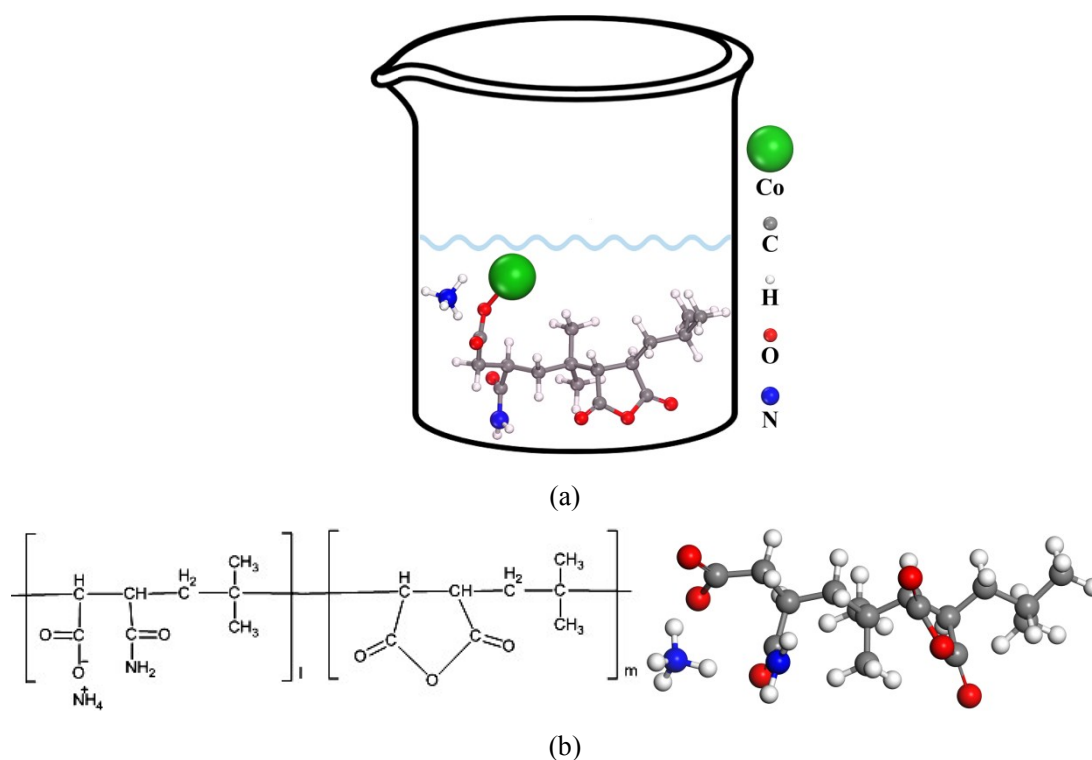
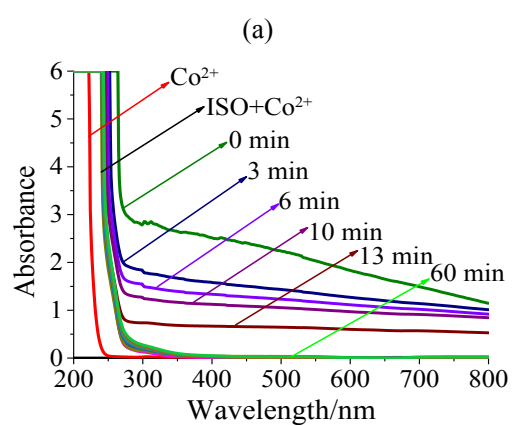
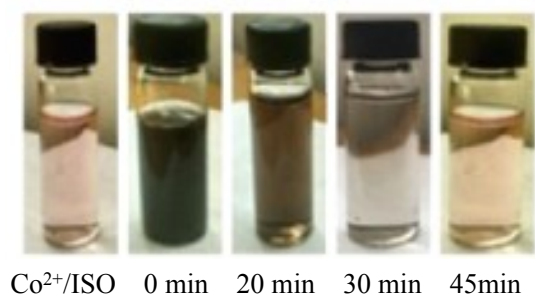
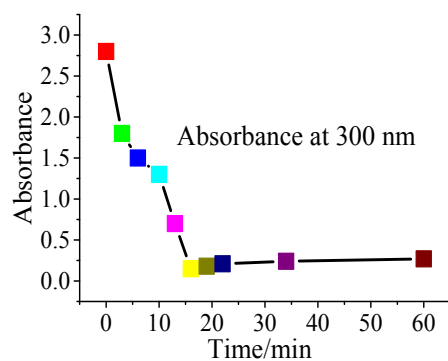


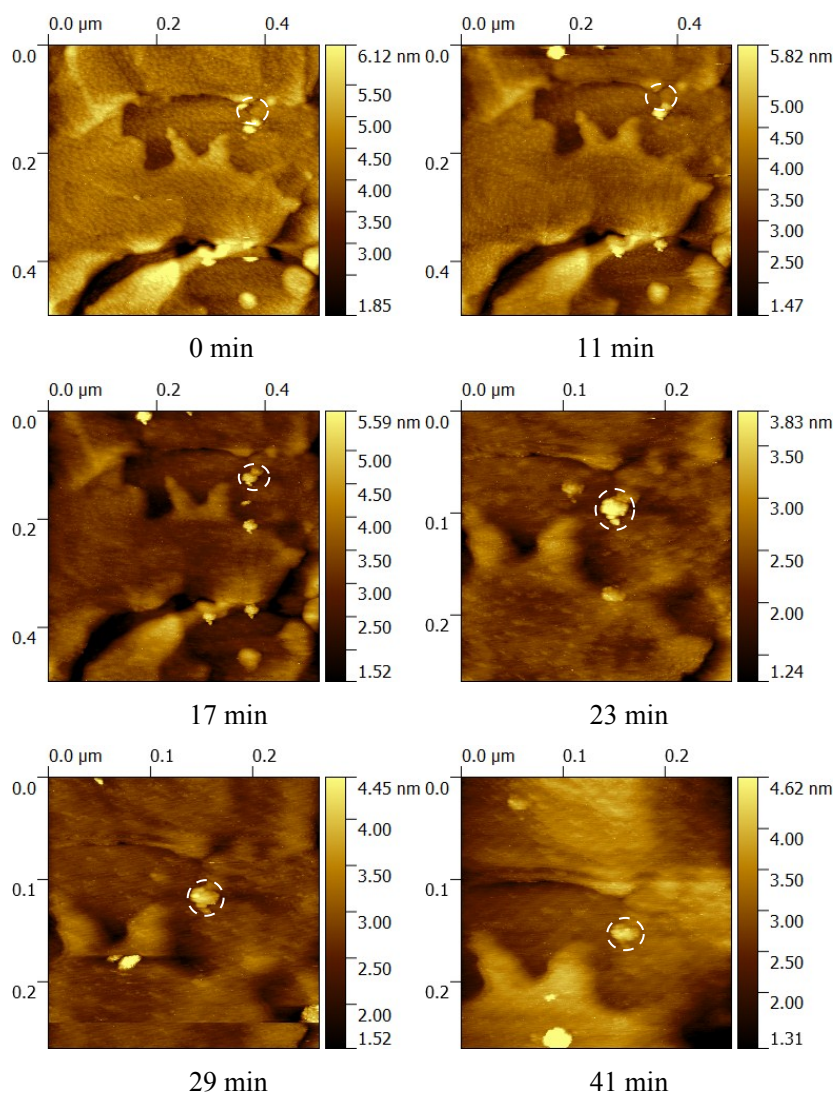
Figure S1(a) The schematic diagram of proposed colloidal single-atom catalysts and (b) The chemical structure of ISOBAM-104.

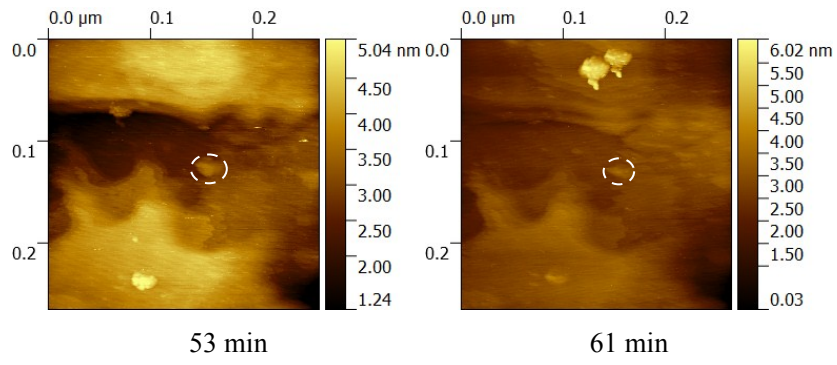




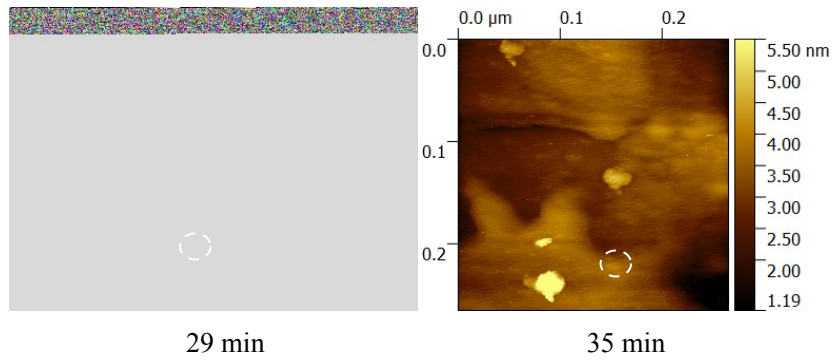
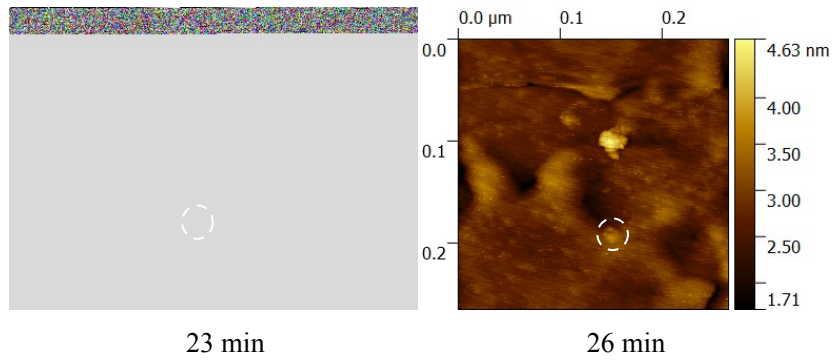
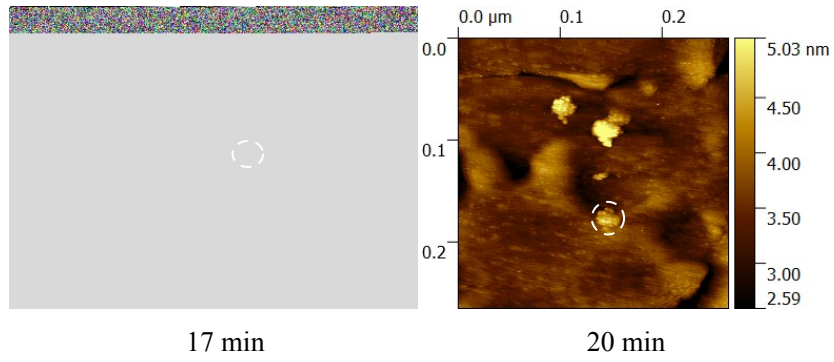
(c)

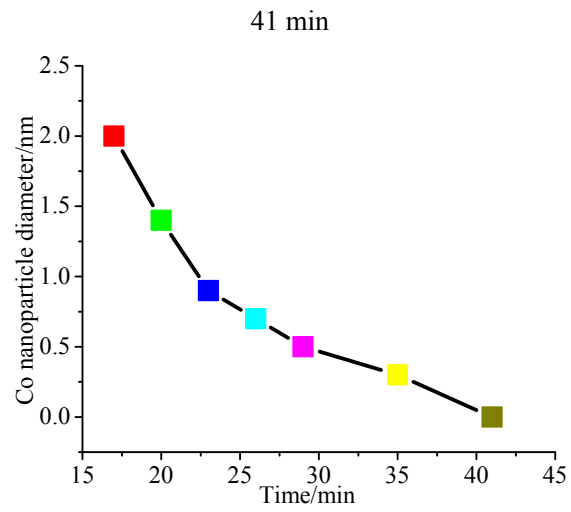
Figure S2 (a) Color evolution of ISOBAM-104 stabilized Co^{2+} solutions before and after reduction in air for various minutes, (b) UV-Vis spectra of Co^{2+} , ISOBAM-104, and ISOBAM-104 stabilized Co^{2+} solutions before and after reduction in air for various minutes, and (c) the UV-Vis absorption intensity of ISOBAM-104 stabilized Co^{2+} at 300 nm after addition of KBH_4 versus storing period. ($[\text{Co}^{2+}] = 0.9 \text{ mM}$, $R_{\text{ISO}} = 40$, $V_{\text{total}} = 50 \text{ mL}$, $30 \text{ }^\circ\text{C}$).



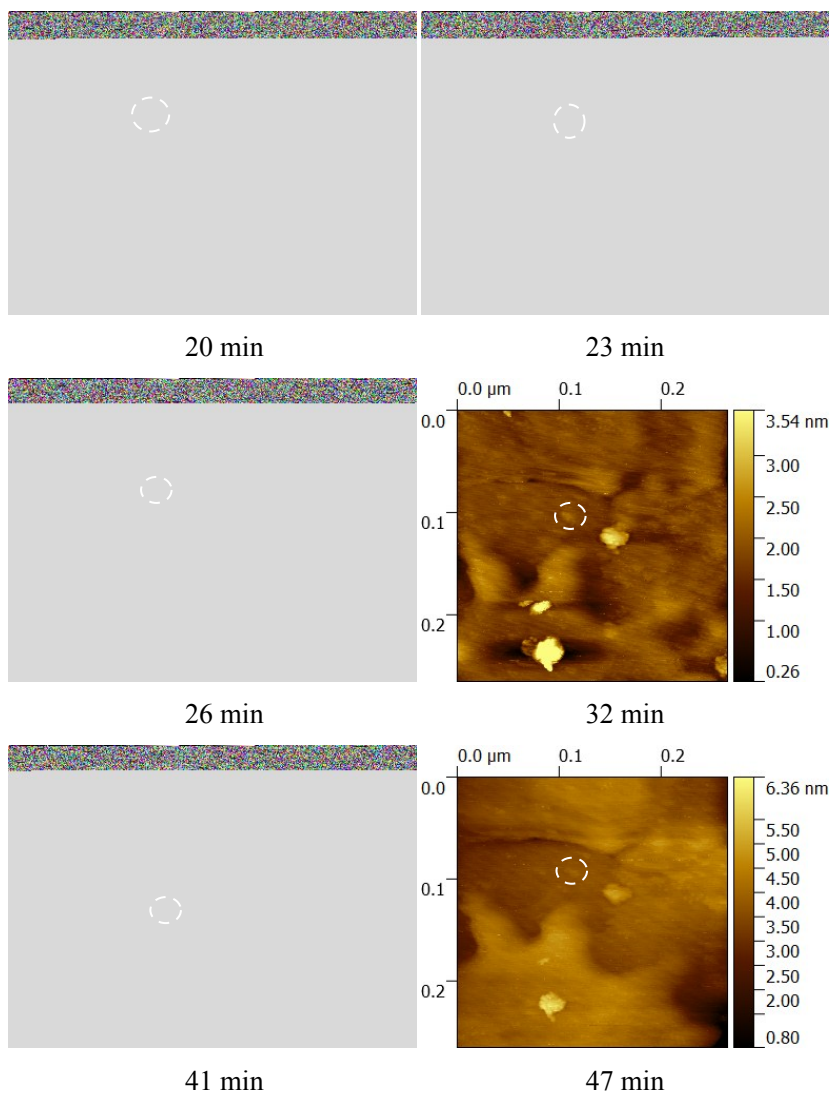


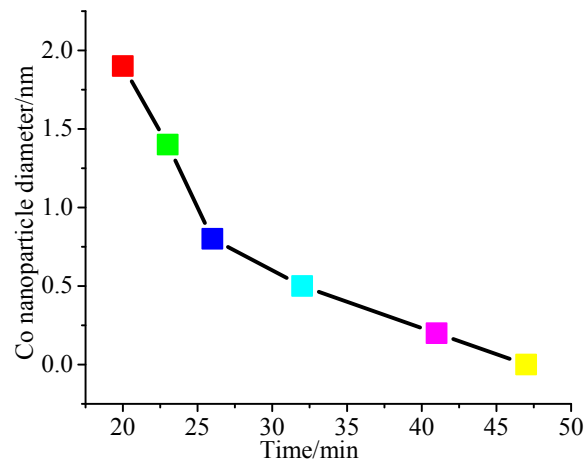
(a) Nanoparticle-1



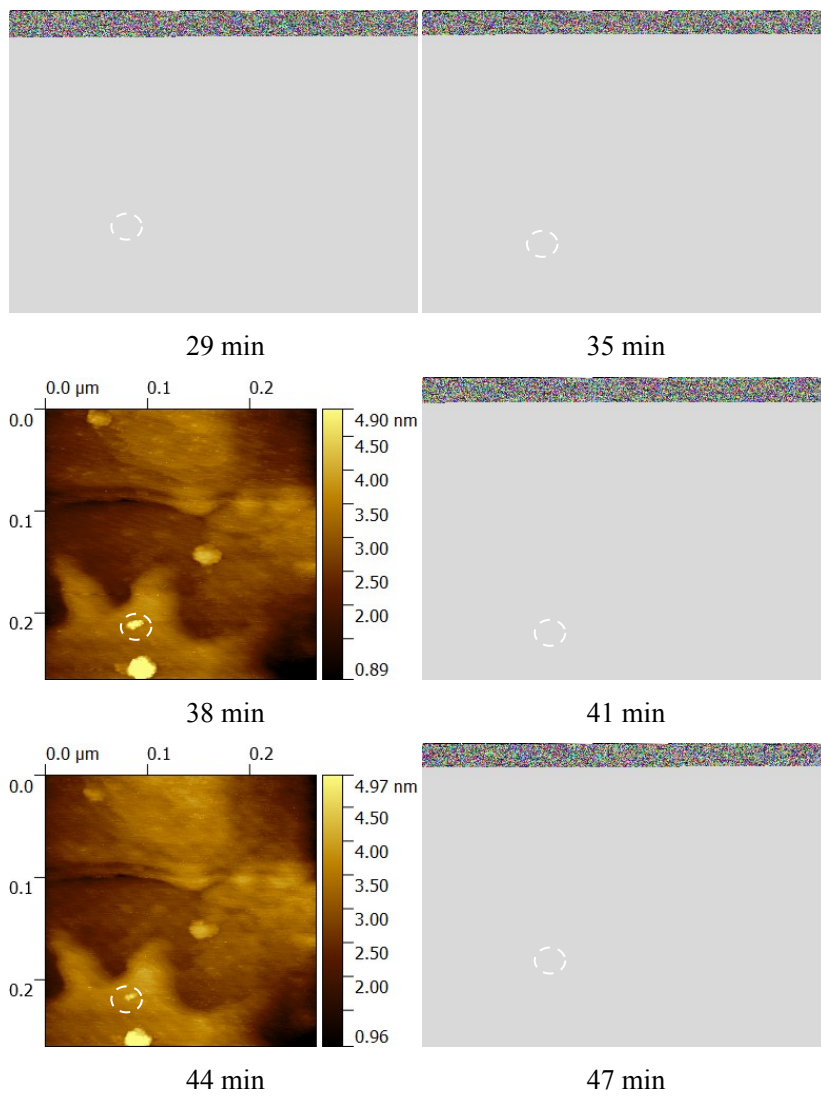


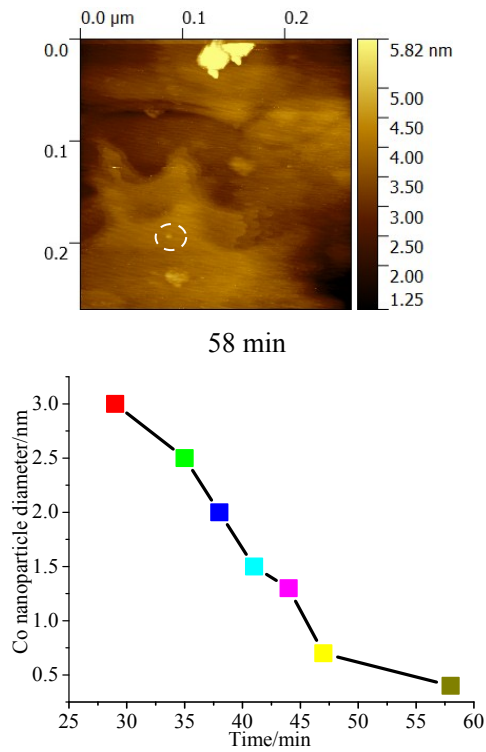
(b) nanoparticle-2



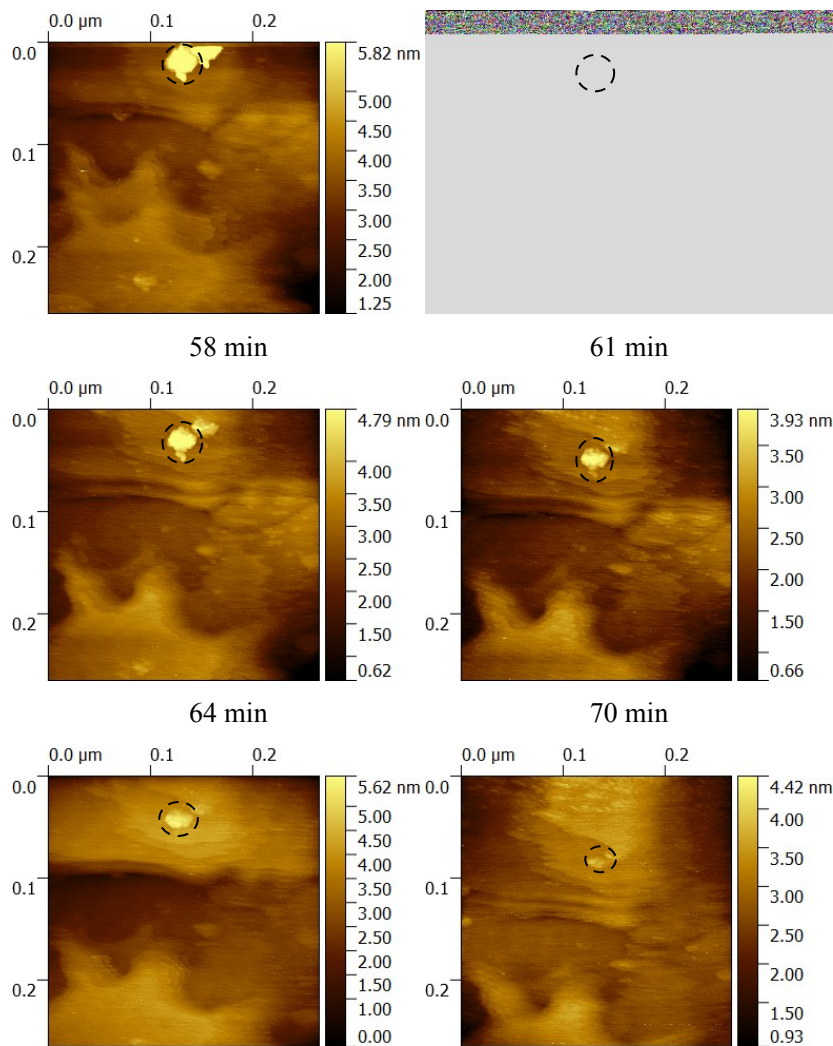


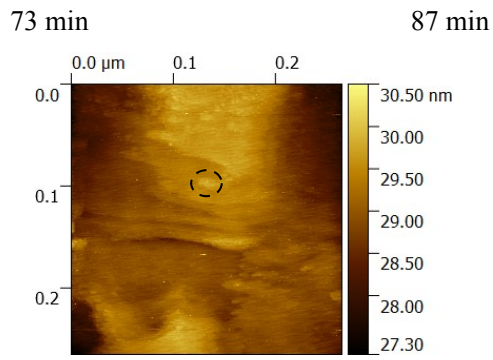
(c) Nanoparticle-3



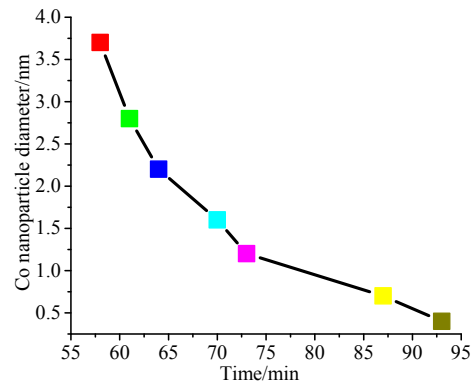


(d) Nanoparticle-4

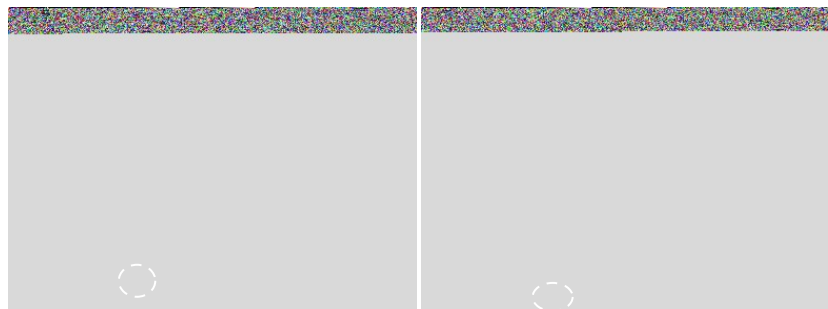




93 min

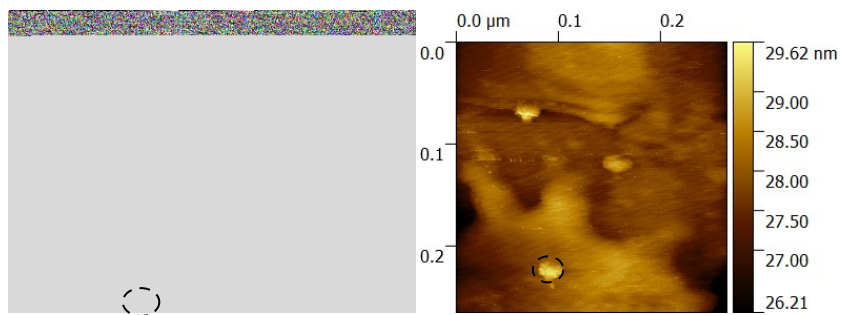


(e) Nanoparticle-5



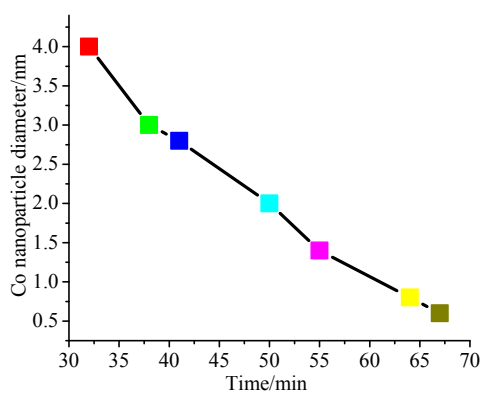
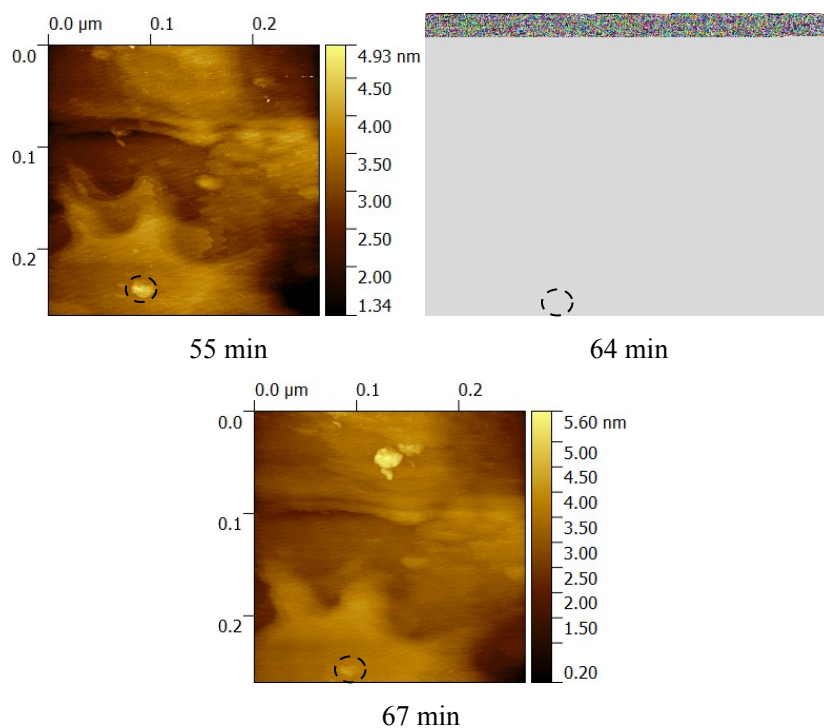
32 min

38 min



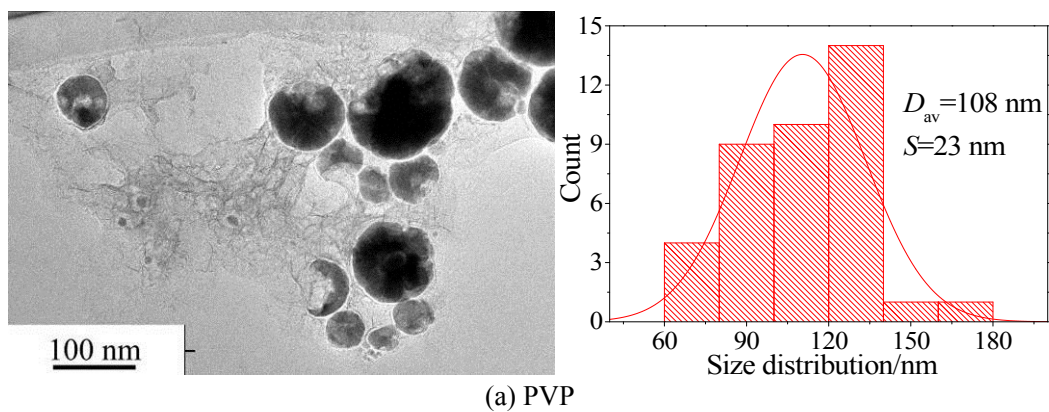
41 min

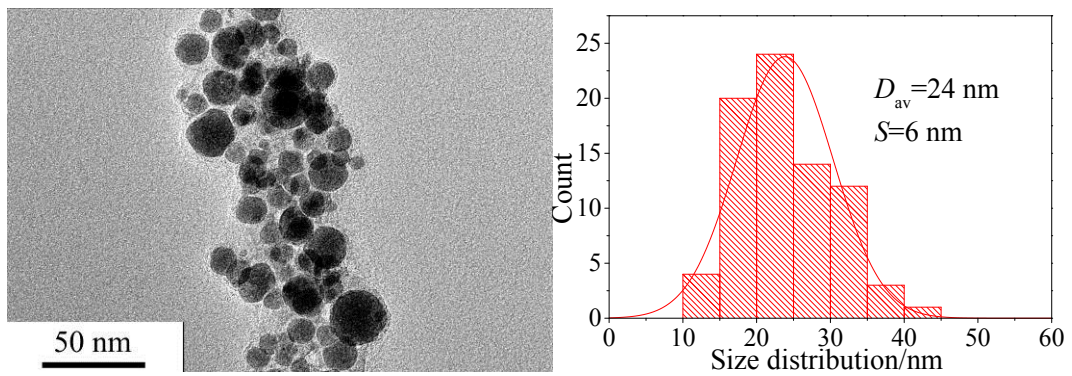
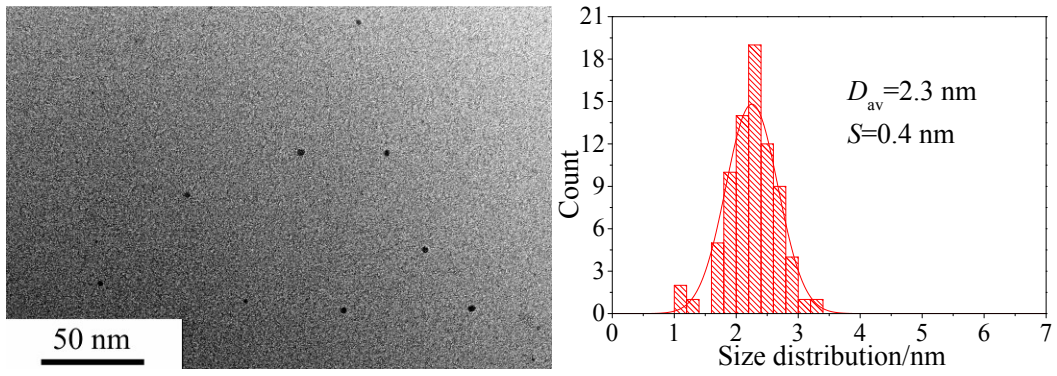
50 min



(f) Nanoparticle-6

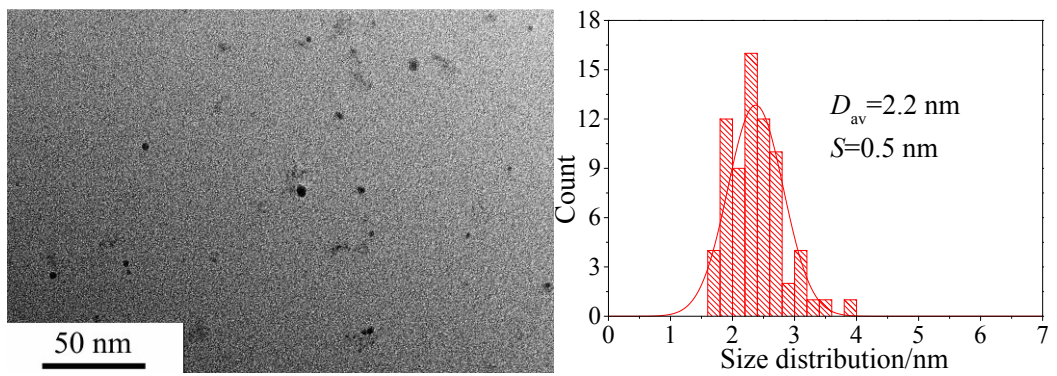
Figure S3 SPM images of ISOBAM-104 protected Co NPs and their size evolution with storing period.



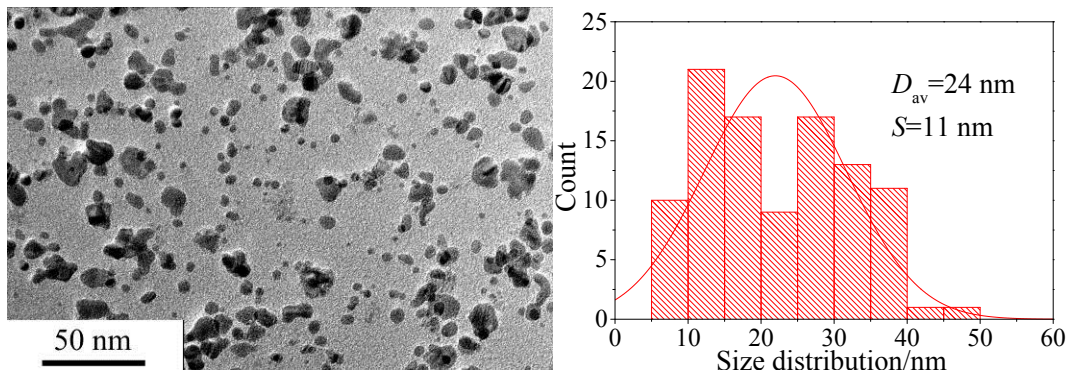


Sediment colloidal NPs

(b) Starch

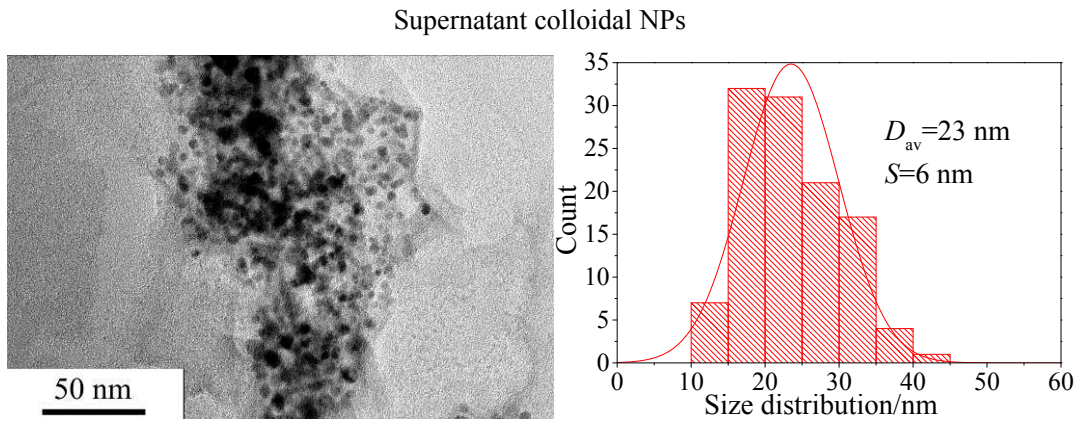
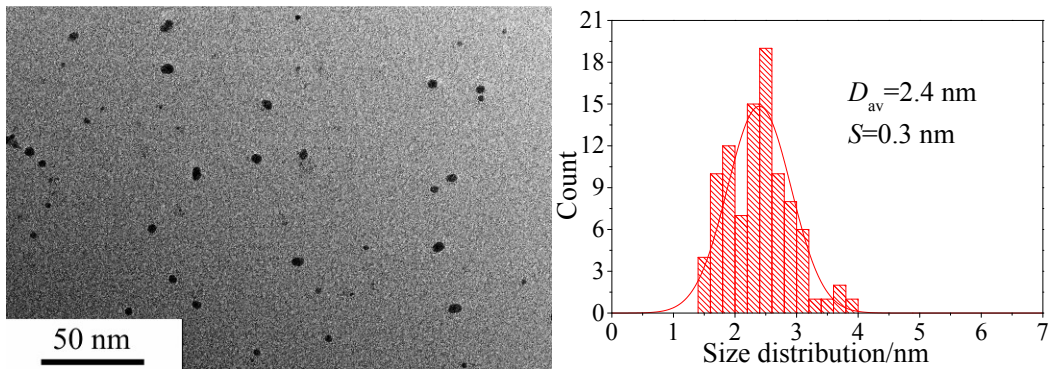


Supernatant colloidal NPs



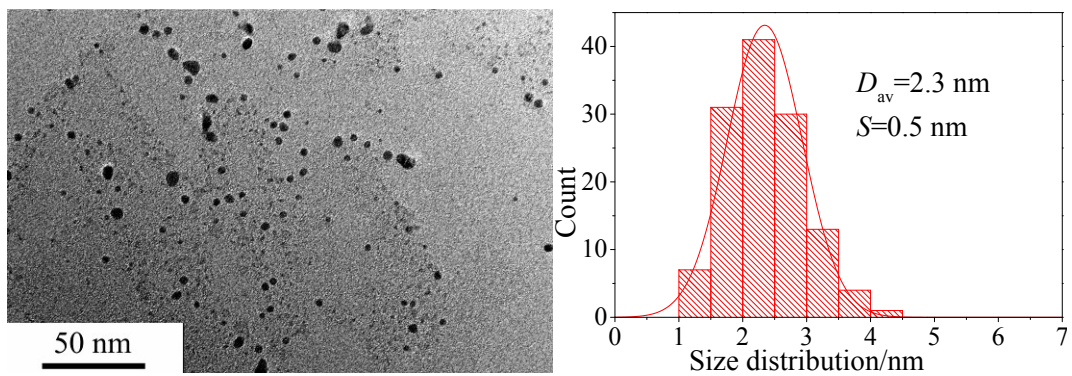
Sediment colloidal NPs

(c) CMC-Na

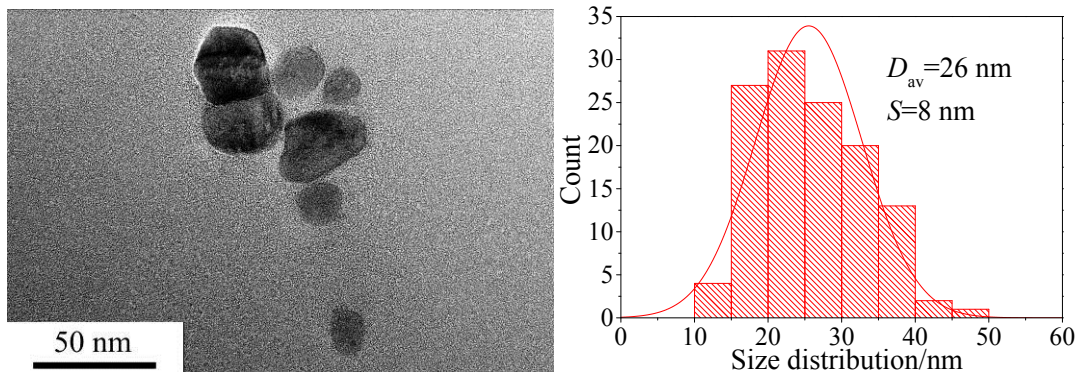


Sediment colloidal NPs

(d) PVA

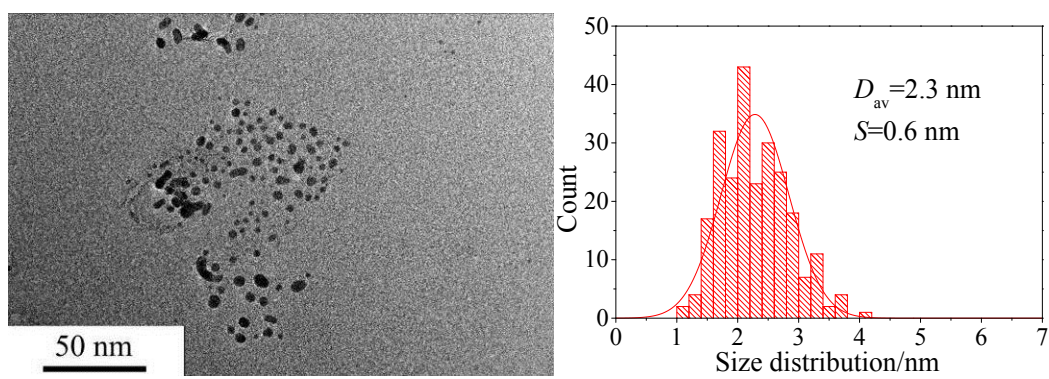


Supernatant colloidal NPs



Sediment colloidal NPs

(e) PAAS



(f) PEG

(D_{av} : average particle size; S : standard deviation)

Figure S4 TEM images and size distribution histograms of Co NPs synthesized with different types of protective agents (Samples both in supernatant and sediment were characterized by TEM for the Co NPs synthesized using PVP, Starch, CMC-Na, PVA, PAAS and PEG as protective agents for comparison.

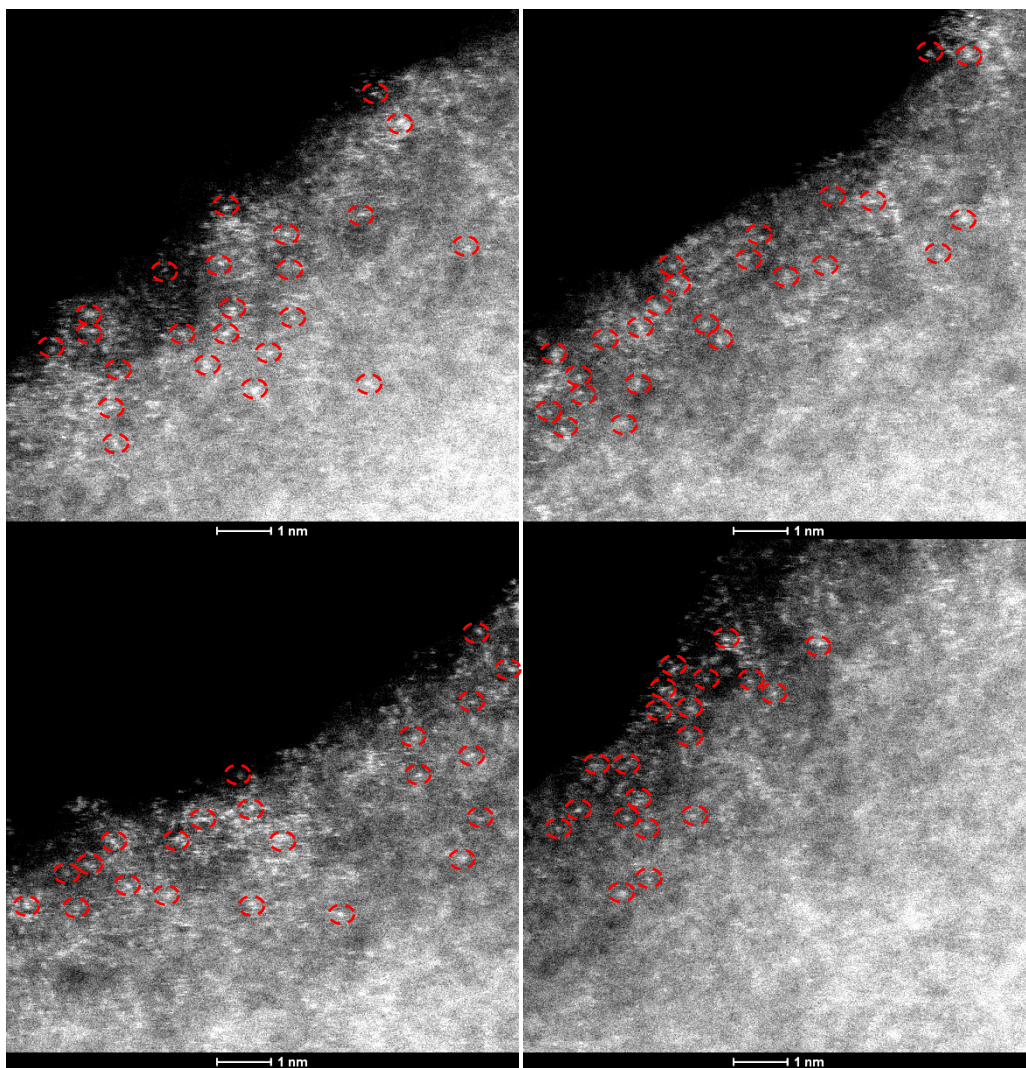
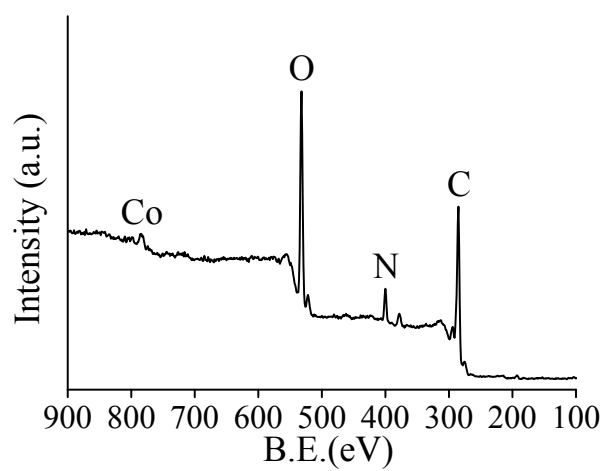
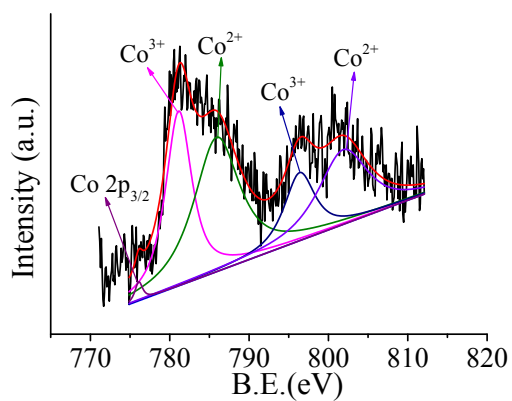


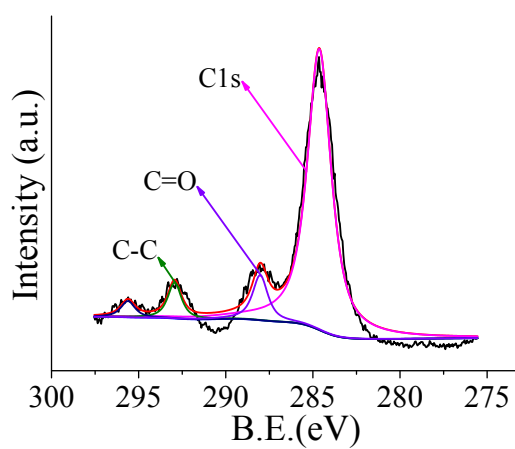
Figure S5 HAADF-STEM images of ISOBAM-104-stabilized colloidal Co catalysts.



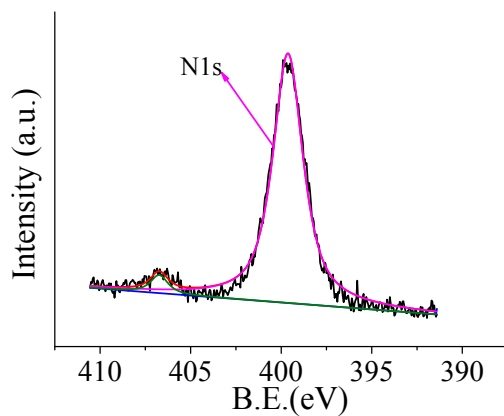
(a) Total Survey XPS spectra



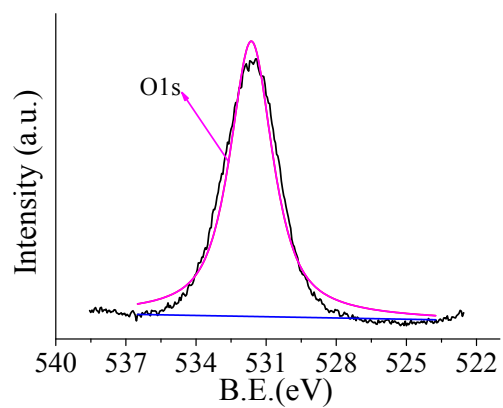
(b) Co XPS spectra



(c) C XPS spectra



(d) N XPS spectra



(e) O XPS spectra

Figure S6 Total survey, Co, C, N and O XPS spectra of ISOBAM-104-protected Co NPs

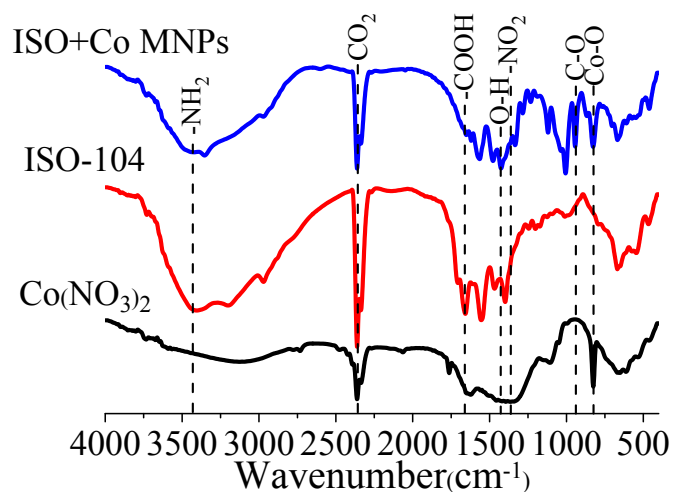
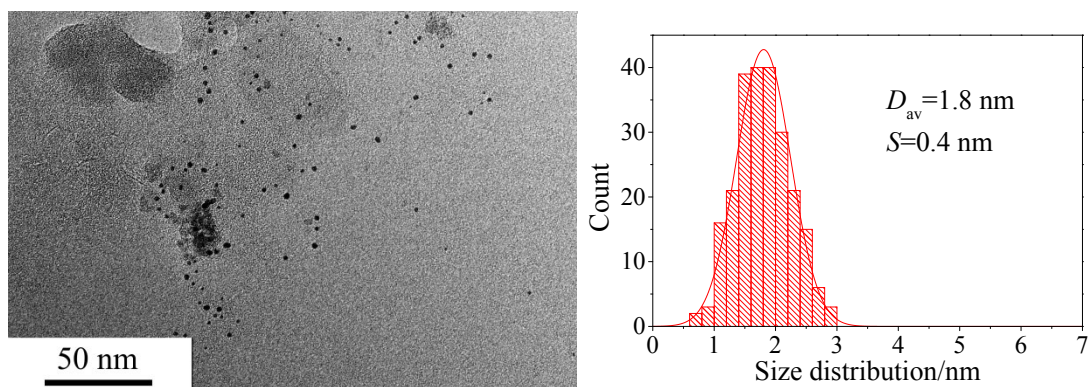
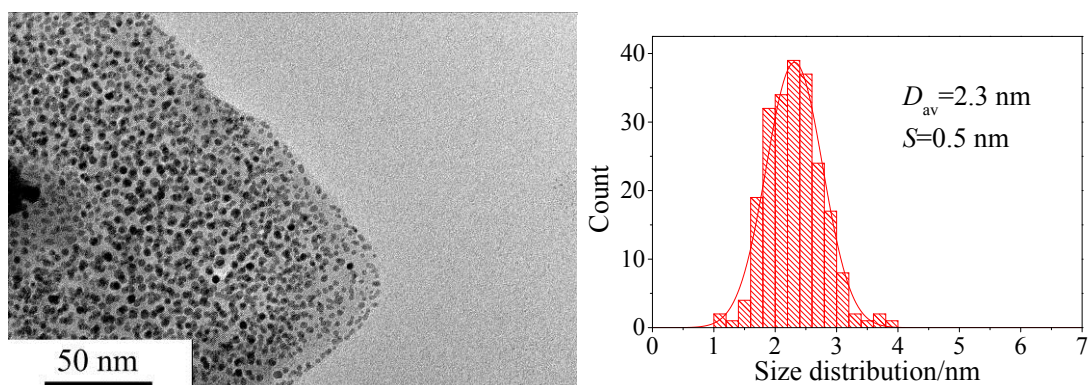


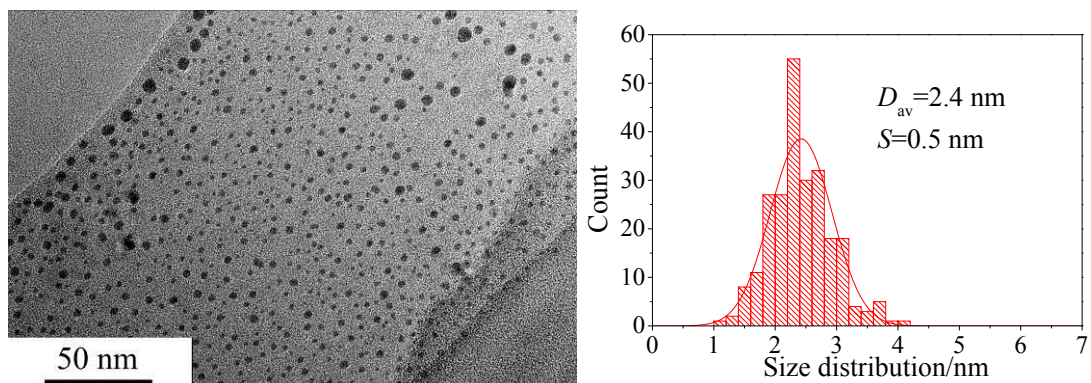
Figure S7 FT-IR spectra of ISOBAM-104, $\text{Co}(\text{NO}_3)_2$ and Co NPs/ISOBAM-104.



(a) Pt NPs



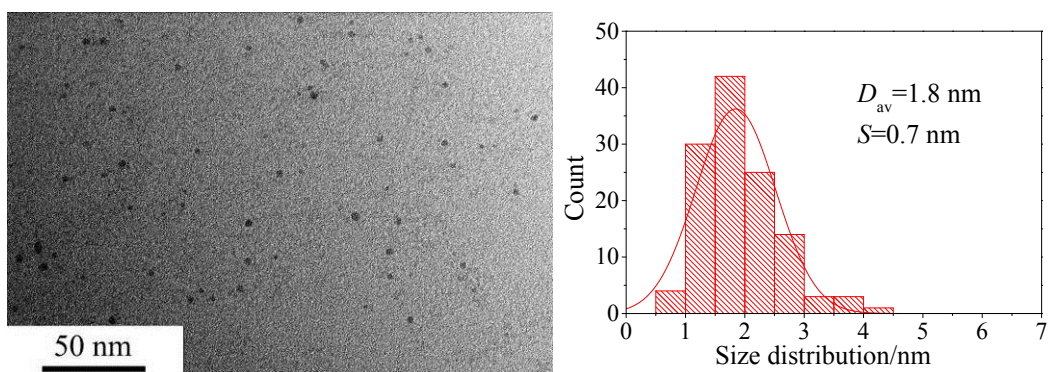
(b) Pd NPs



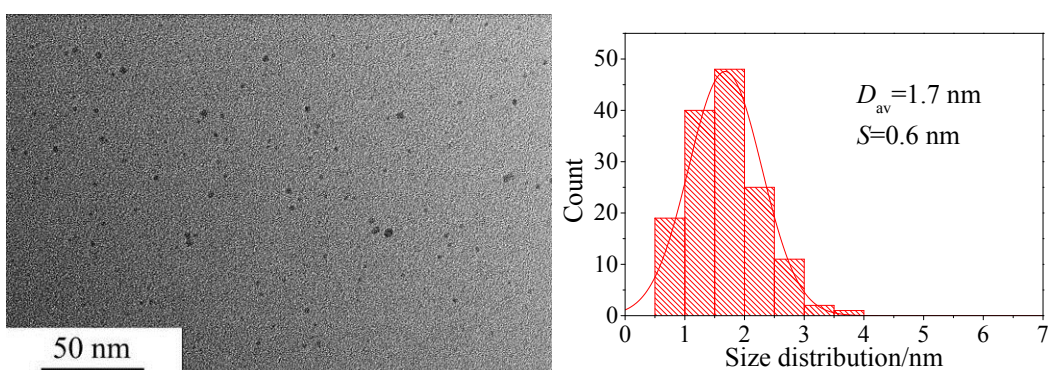
(c) Rh NPs

(D_{av} : average particle size; S : standard deviation)

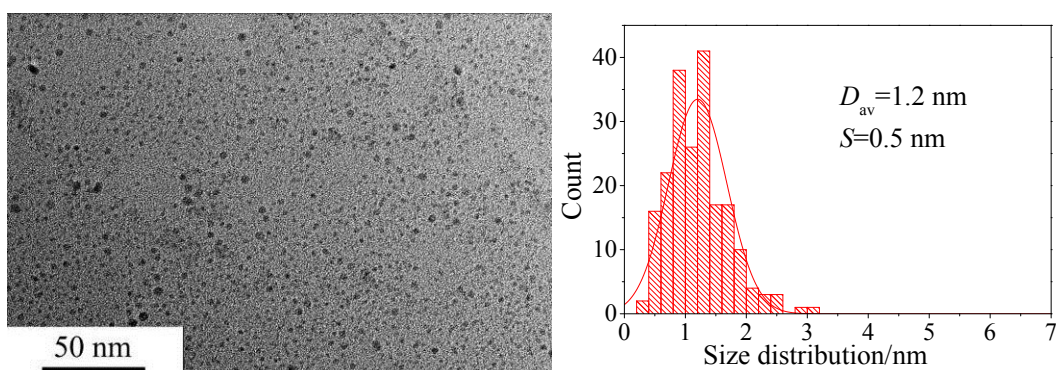
Figure S8 TEM images and size distribution histograms of ISOBAM-104 protected Pt, Pd and Rh NPs.



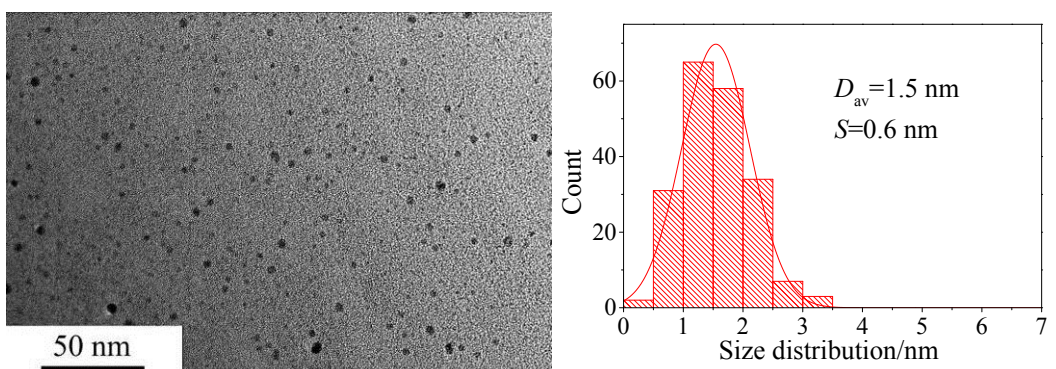
(a) $R_{ISO}=20$



(b) $R_{ISO}=30$



(c) $R_{ISO}=40$



(d) $R_{ISO}=50$

(D_{av} : average particle size; S : standard deviation)

Figure S9 TEM images and size distribution histograms of Co NPs synthesized with various R_{ISO} values ($[Co^{2+}] = 0.6 \text{ mM}$, $V_{total} = 50 \text{ mL}$, $30 \text{ }^\circ\text{C}$).

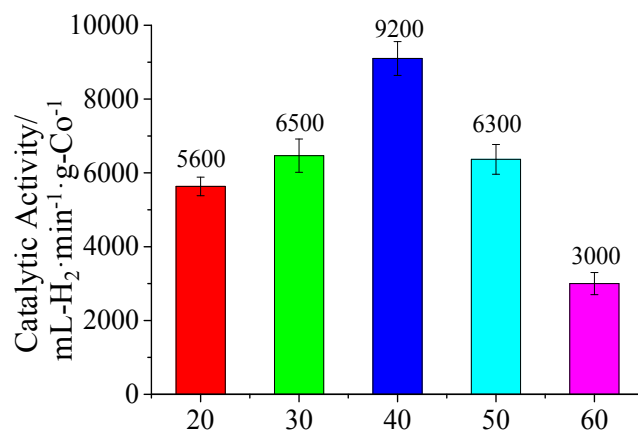
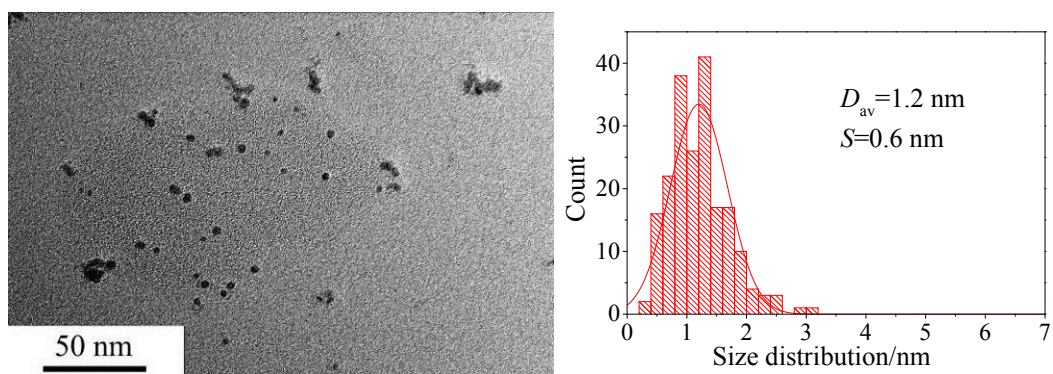
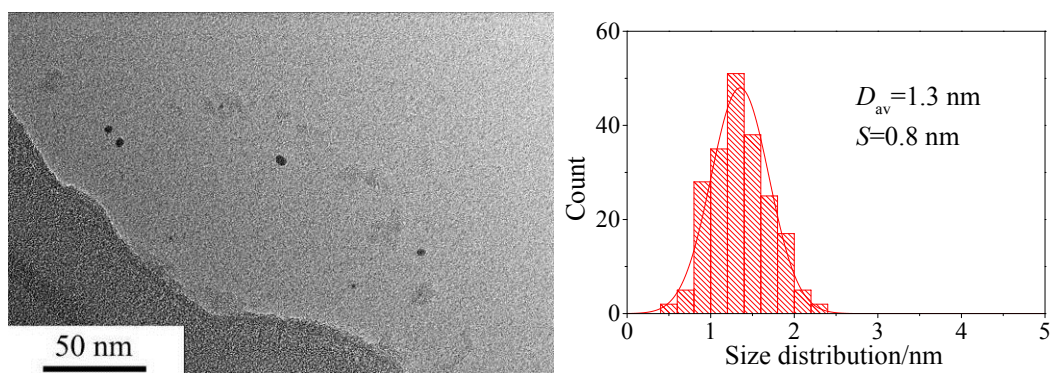


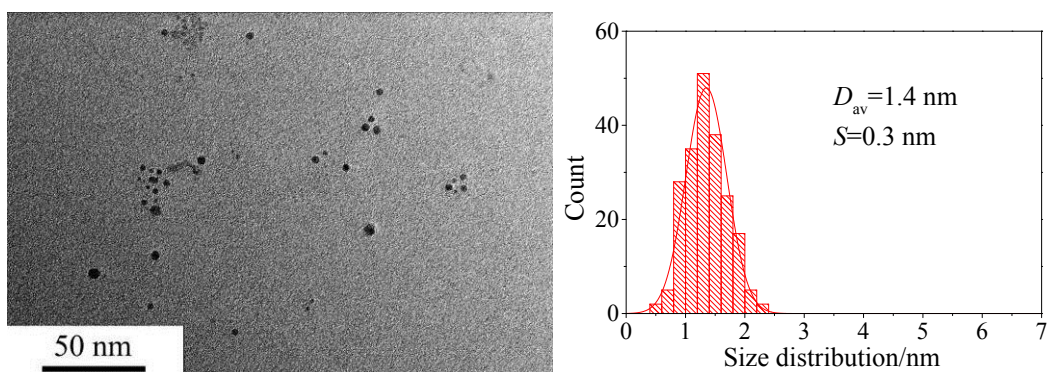
Figure S10 Intrinsic catalytic activity of Co NPs synthesized with various R_{ISO} values using $\text{Co}(\text{NO}_3)_2 \cdot 6\text{H}_2\text{O}$ as precursor ($[\text{Co}^{2+}] = 0.6 \text{ mM}$, $V_{\text{total}} = 50 \text{ mL}$, $30 \text{ }^\circ\text{C}$).



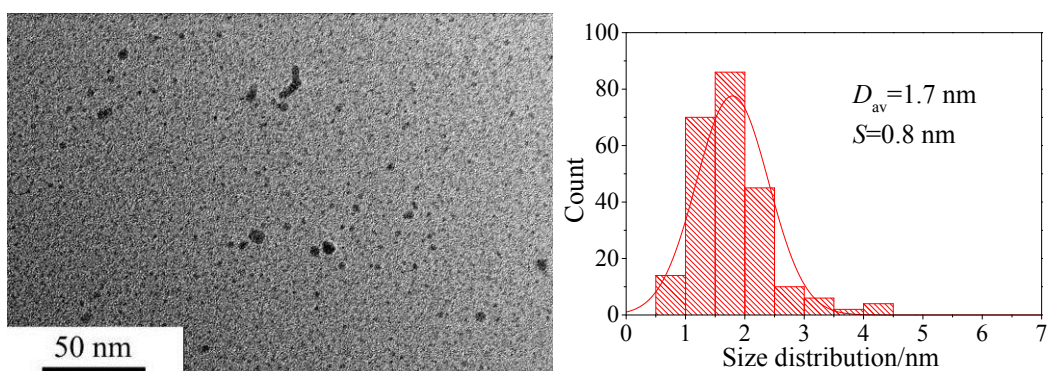
(a) $[\text{Co}^{2+}] = 0.6 \text{ mM}$



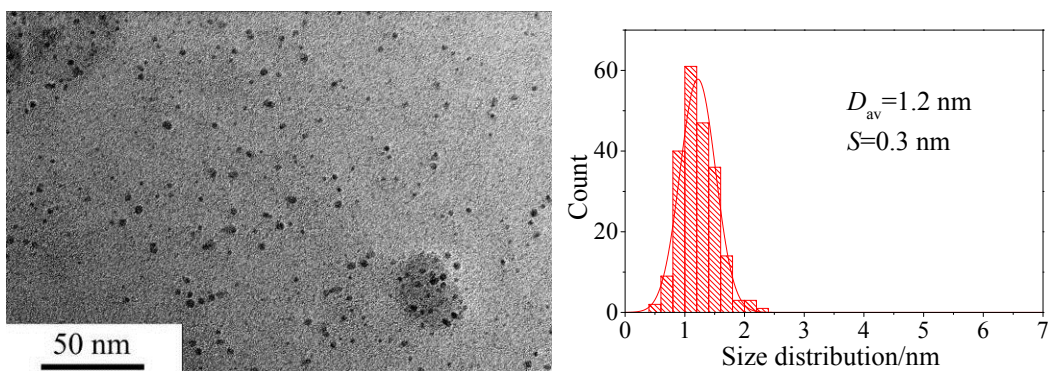
(b) $[\text{Co}^{2+}] = 0.75 \text{ mM}$



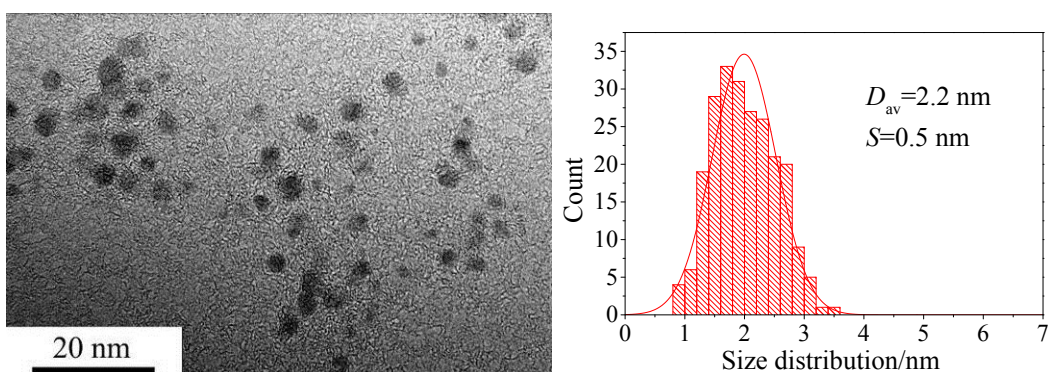
(c) $[Co^{2+}] = 0.9 \text{ mM}$



(d) $[Co^{2+}] = 1.2 \text{ mM}$



(e) $[Co^{2+}] = 1.5 \text{ mM}$



(f) $[Co^{2+}] = 1.8 \text{ mM}$

(D_{av} : average particle size; S : standard deviation)

Figure S11 TEM images and size distribution histograms of Co NPs synthesized with various $Co(NO_3)_2 \cdot 6H_2O$ concentrations ($R_{ISO} = 40$, $V_{total} = 50 \text{ mL}$, $30 \text{ }^\circ\text{C}$).

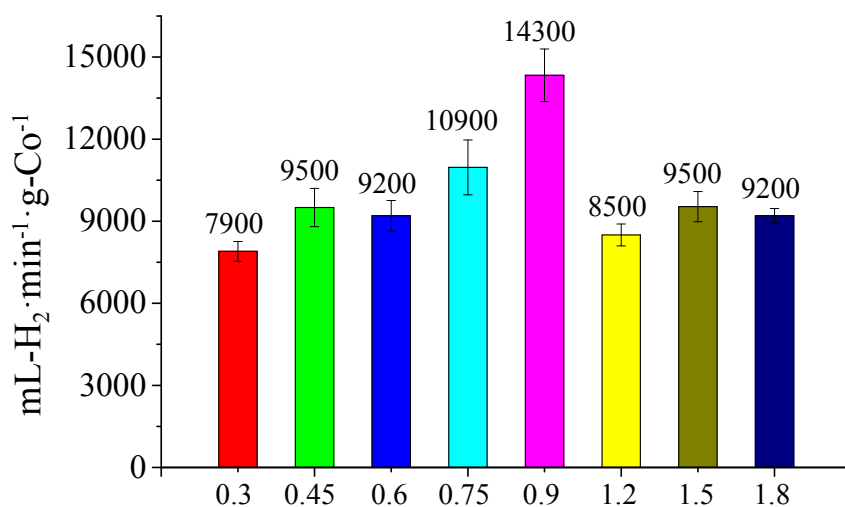


Figure S12 Intrinsic catalytic activity of Co NPs synthesized at various Co²⁺ concentrations ($R_{\text{ISO}}=40$, $V_{\text{total}}=50$ mL, 30 °C).

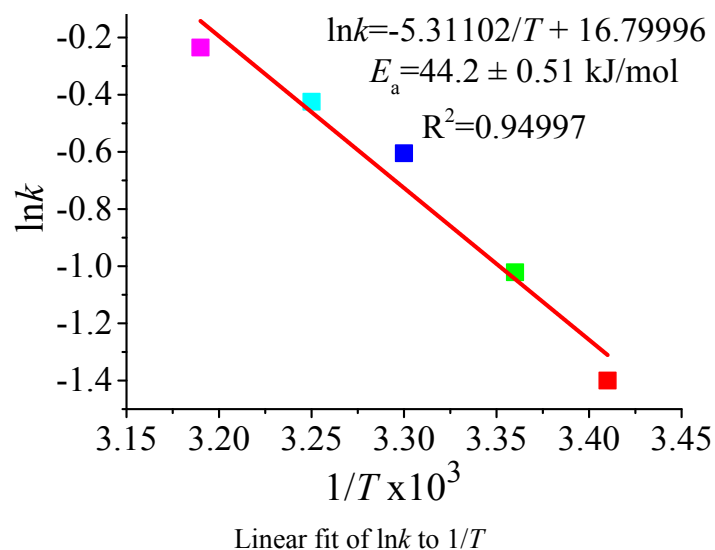
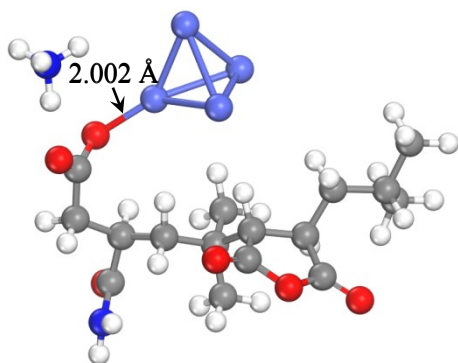
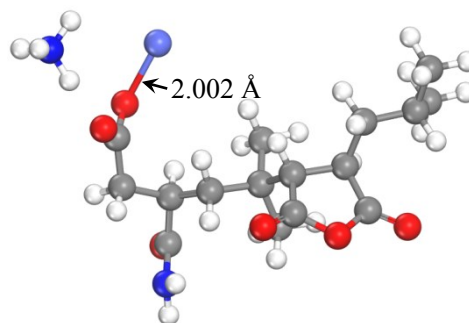


Figure S13 Effect of temperature on the catalytic performance of Co NPs: Linear fit of $\ln k$ vs. $1/T$ ($[\text{Co}^{2+}] = 0.9$ mM, $R_{\text{ISO}} = 40$, $V_{\text{total}} = 50$ mL, 30 °C).



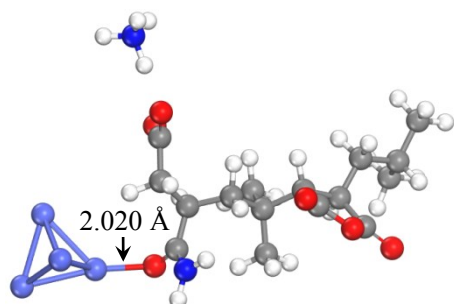
binding energy: -232.1kJ/mol

(a1) Co₄ cluster on COO⁻ site of ISOBAM-104



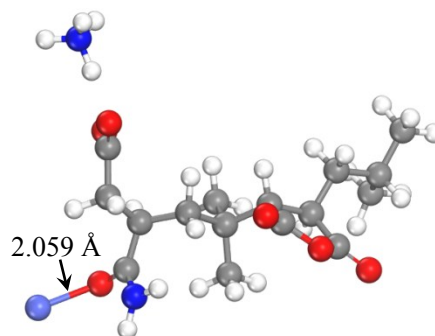
binding energy: -191.7kJ/mol

(b1) Co single atom on COO⁻ site of ISOBAM-104



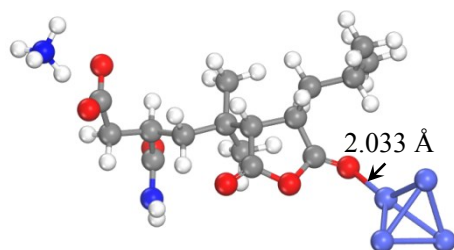
binding energy: -198.2 kJ/mol

(a2) Co₄ cluster on CONH₂ site of ISOBAM-104



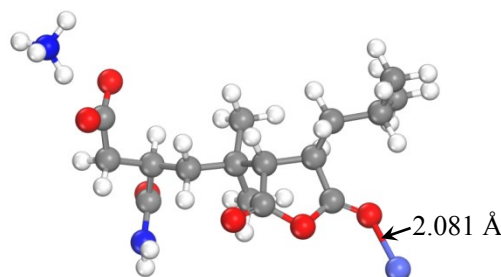
binding energy: 180.6 kJ/mol

(b2) Co single atom on CONH₂ site of ISOBAM-104



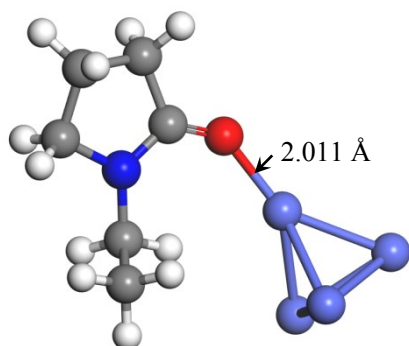
binding energy: -188.4 kJ/mol

(a3) Co₄ cluster on OCOCO site of ISOBAM-104



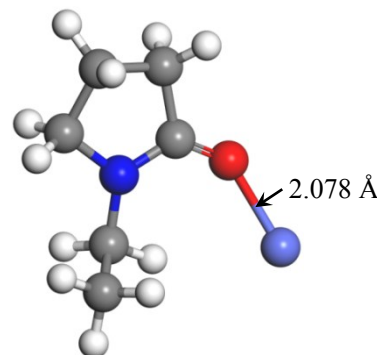
binding energy: -173.5 kJ/mol

(b3) Co single atom on OCOCO site of ISOBAM-104



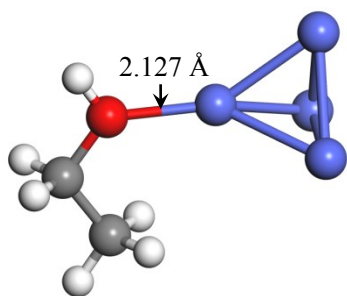
binding energy: -113.1 kJ/mol

(a4) Co₄ cluster on PVP



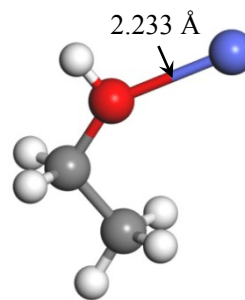
binding energy: -91.1 kJ/mol

(b4) Co single atom on PVP



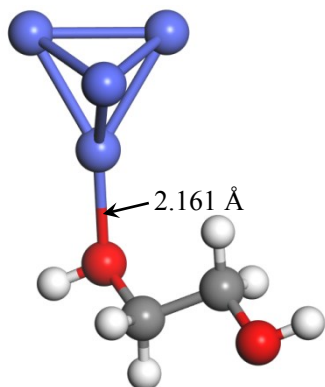
binding energy: -62.5 kJ/mol

(a5) Co₄ cluster on PVA



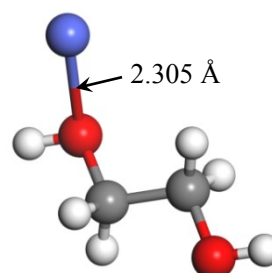
binding energy: -42.3 kJ/mol

(b5) Co single atom on PVA



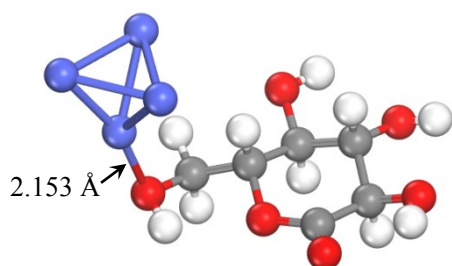
binding energy: -72.7 kJ/mol

(a6) Co₄ cluster on PEG



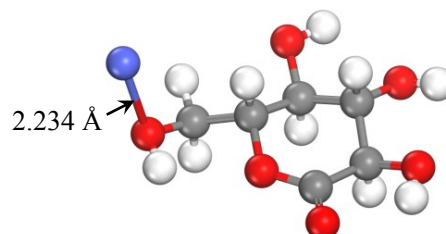
binding energy: -52.6 kJ/mol

(b6) Co single atom on PEG



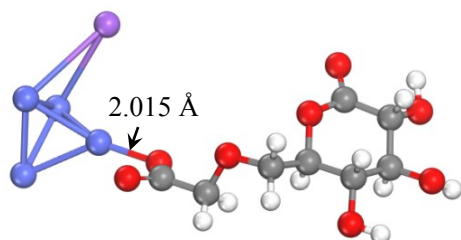
binding energy: -108.2 kJ/mol

(a7) Co₄ cluster on Starch



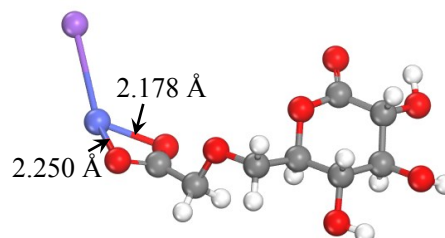
binding energy: -91.1 kJ/mol

(b7) Co single atom on Starch



binding energy: -91.0 kJ/mol

(a8) Co₄ cluster on CMC-Na



binding energy: -42.4 kJ/mol

(b8) Co single atom on CMC-Na

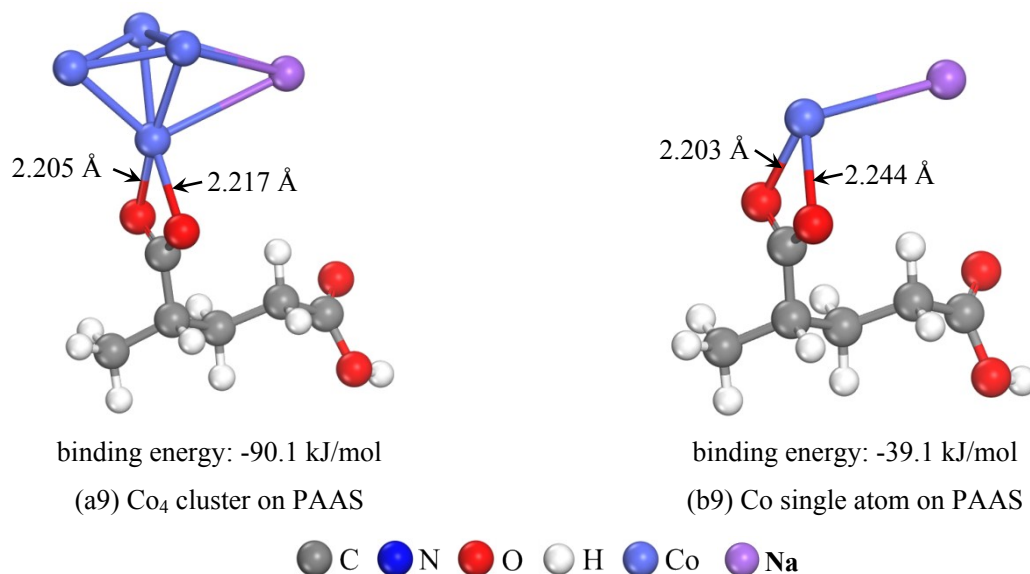


Figure S14 Geometric structures and binding energies of Co₄ cluster and Co single atom on various stabilizing agents.

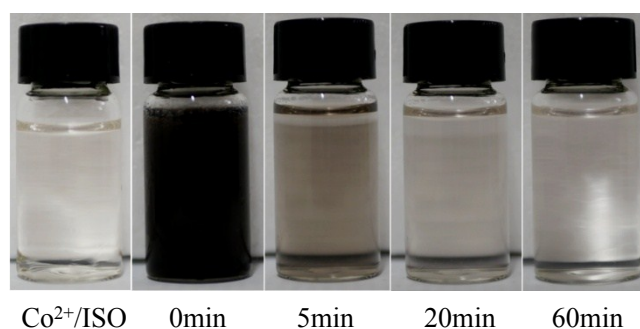


Figure S15 Color evolution of CMC-NH₄ (Ammonium Carboxy Methyl Cellulose) stabilized Co²⁺ solutions before and after reduction in air for various periods. ([Co²⁺]=0.9 mM, $R_{\text{CMC-NH}_4}$ =40, V_{total} =50 mL, 30 °C).

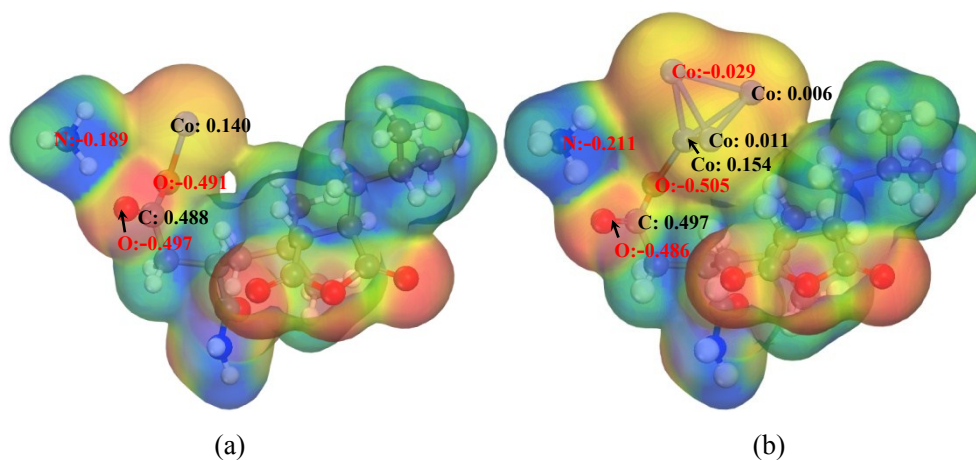
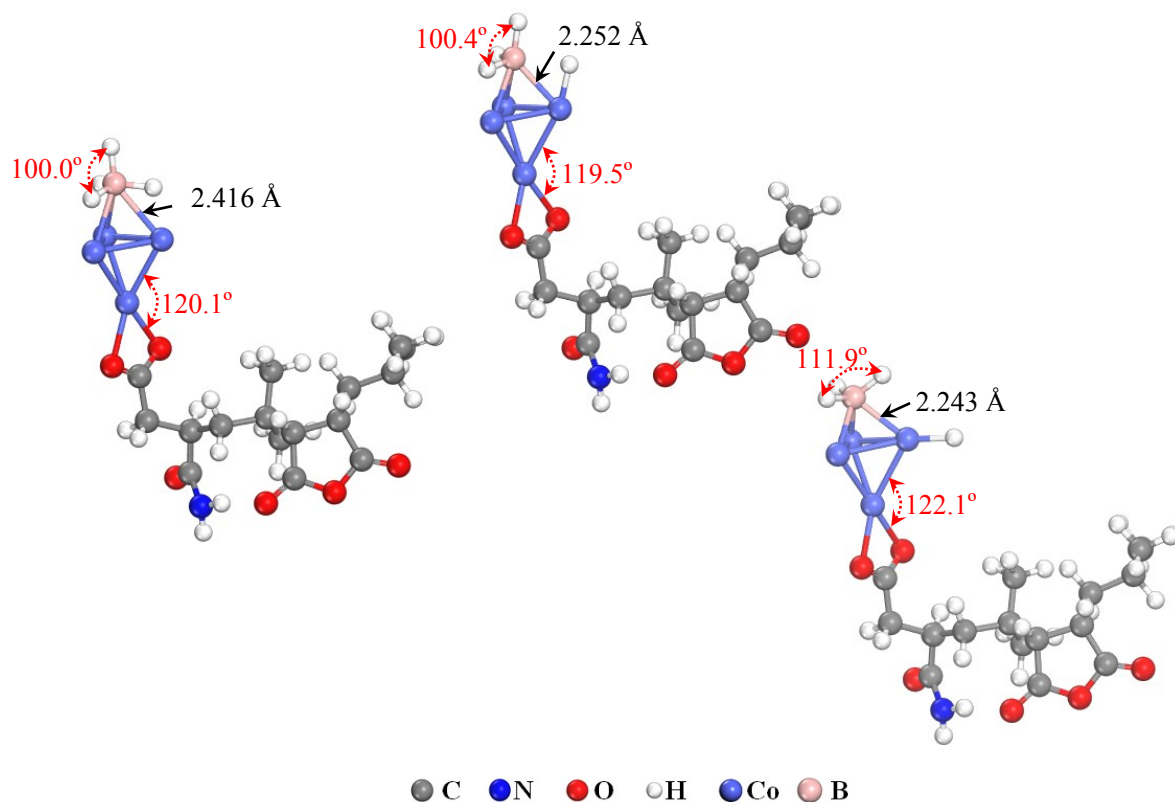
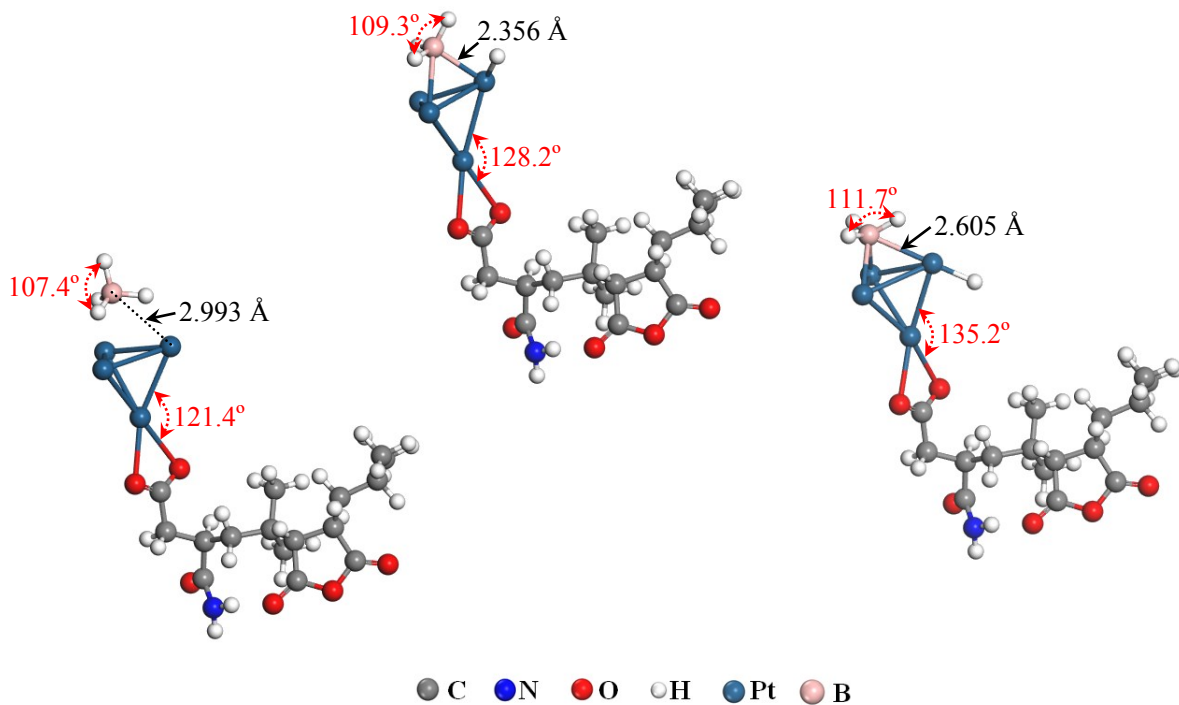


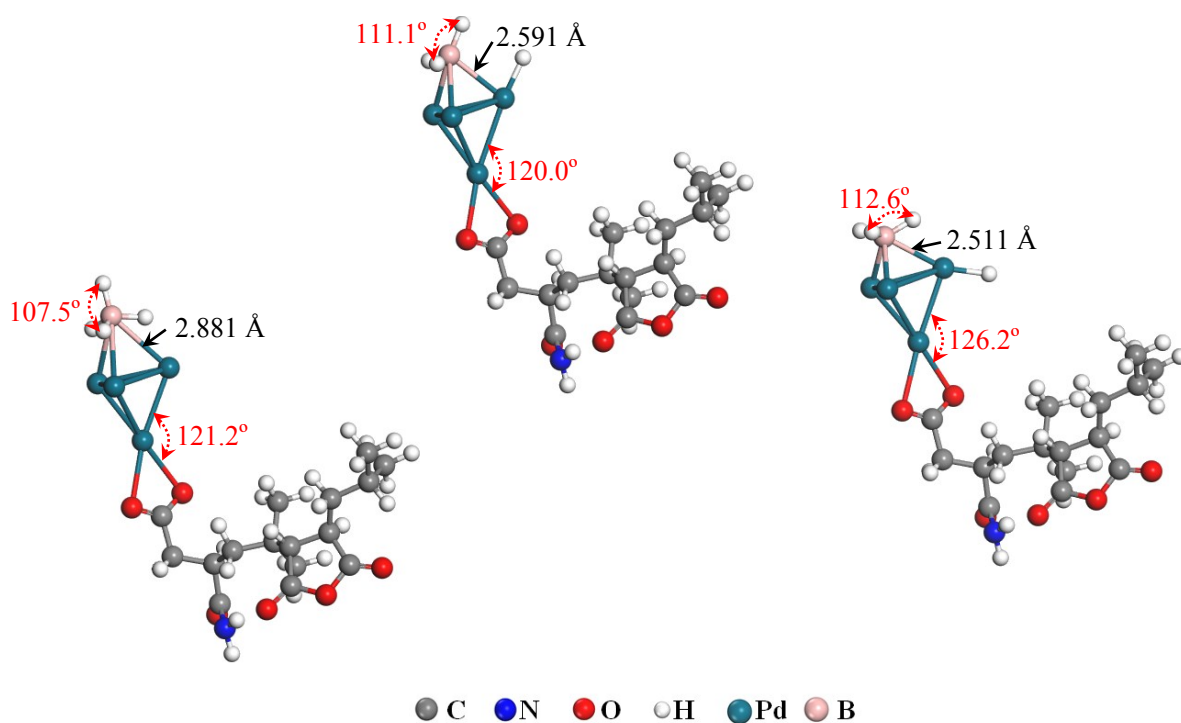
Figure S16 Differential charge density and Mulliken charges of (a) Co single atom and (b) Co₄ cluster on ISOBAM-104.



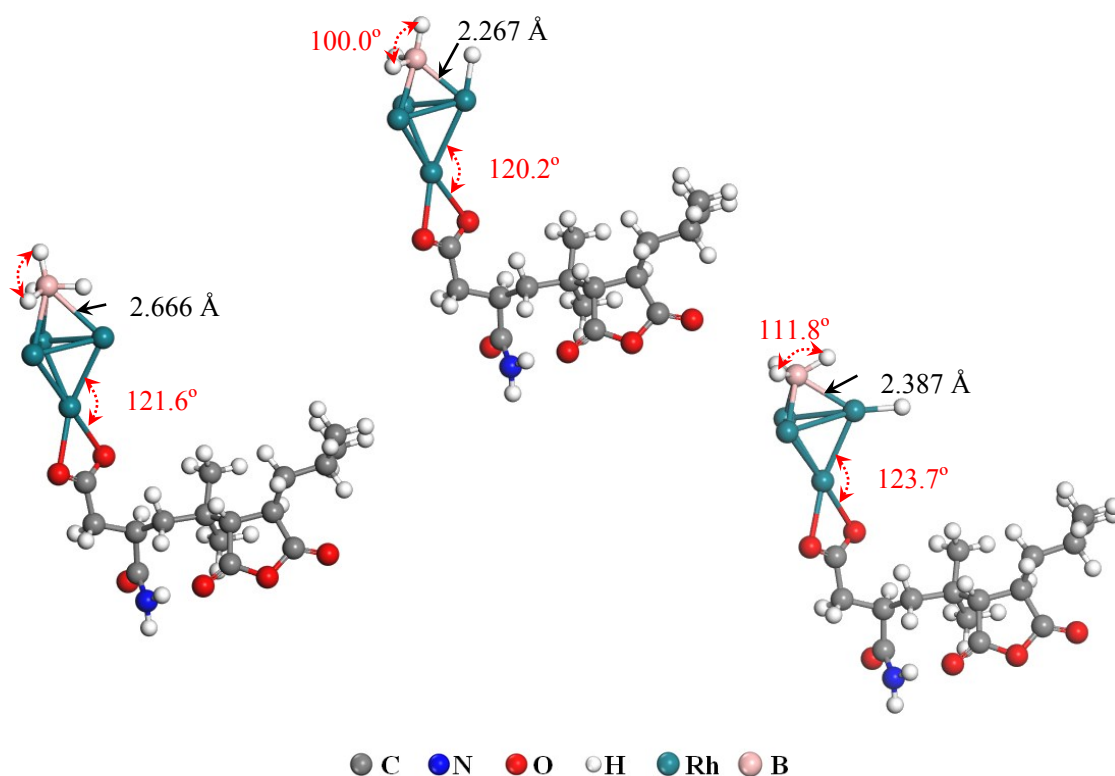
(a) The first elementary step in the borohydride hydrolysis catalyzed by Co₄-ISO



(b) The first elementary step in the borohydride hydrolysis catalyzed by Pt₄-ISO



(c) The first elementary step in the borohydride hydrolysis catalyzed by Pd₄-ISO



(d) The first elementary step in the borohydride hydrolysis catalyzed by Rh₄-ISO

Figure S17 Geometric structures of the first elementary step of the borohydride hydrolysis catalyzed by Co₄-ISO, Pt₄-ISO, Pd₄-ISO and Rh₄-ISO.

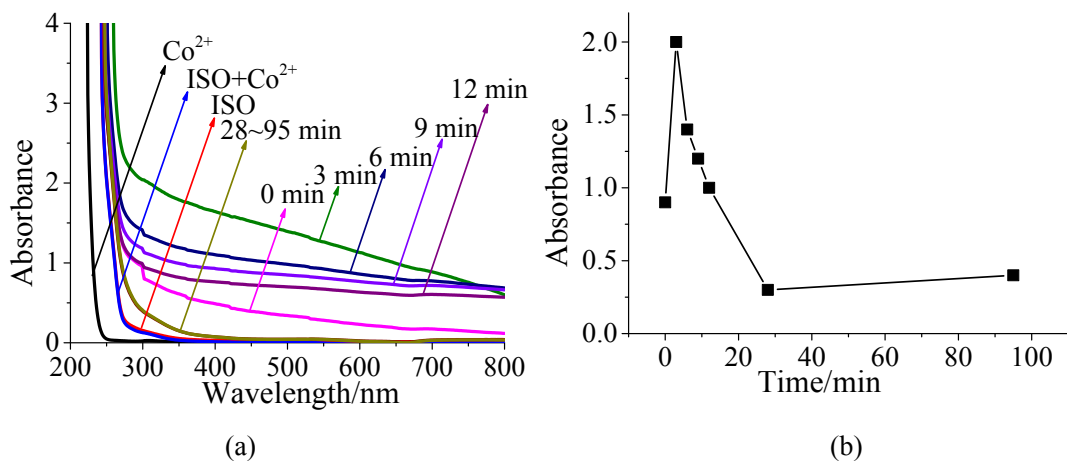


Figure S18 (a) UV-Vis spectra of Co^{2+} , ISOBAM-104, and ISOBAM-104 stabilized Co^{2+} solutions at “second addition” of KBH_4 in air for various minutes, and (b) the UV-Vis absorption intensity of ISOBAM-104 stabilized Co^{2+} at 300 nm at “second addition” of KBH_4 versus storing period. ($[\text{Co}^{2+}] = 0.9 \text{ mM}$, $R_{\text{ISO}} = 40$, $V_{\text{total}} = 50 \text{ mL}$, $30 \text{ }^\circ\text{C}$).

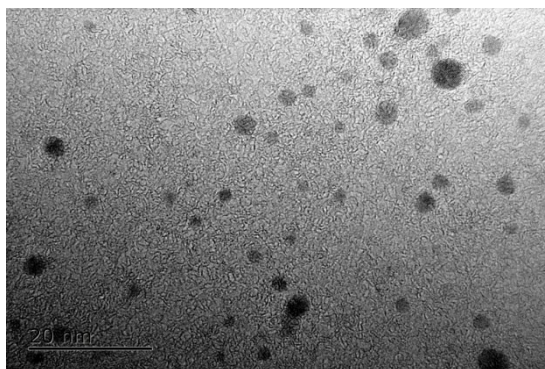


Figure S19 TEM images of Co NPs synthesized at “second addition” of KBH_4 ($R_{\text{ISO}} = 40$, $[\text{Co}^{2+}] = 0.9 \text{ mM}$, $V_{\text{total}} = 50 \text{ mL}$, $30 \text{ }^\circ\text{C}$).

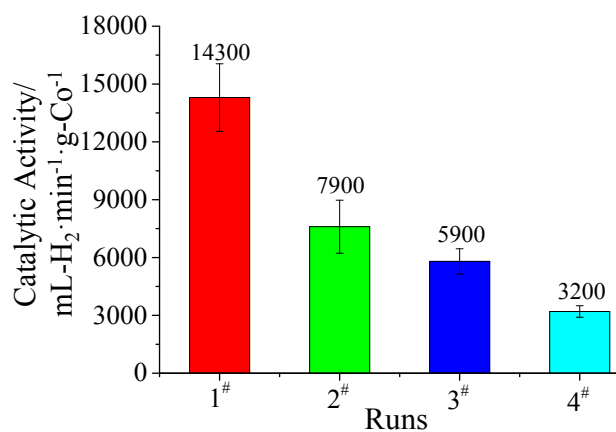


Figure S20 Catalytic durability of as-prepared Co colloidal catalysts: intrinsic catalytic activity of Co NPs ($[\text{Co}^{2+}] = 0.9 \text{ mM}$, $R_{\text{ISO}} = 40$, $V_{\text{total}} = 50 \text{ mL}$, $30 \text{ }^\circ\text{C}$).

Table S1 Catalytic activity of various catalysts in hydrogen generation from hydrolysis of borohydride.

Catalyst	Reactant	Catalytic Activity (mL H ₂ /min/g _{catalyst})	Ref.
Co	KBH ₄	14300	This work
NH ₄ Cl (ammonium species)	KBH ₄	4500	[1]
Ru/Ni foam	NaBH ₄	23030	[2]
Co ₃ O ₄ hollow fiber composed of nanoparticles array	NaBH ₄	11120	[3]
Ni-based complex catalyst supported on Al ₂ O ₃	NaBH ₄	625	[4]
Polymer supported Ni- Schiff Base complex	NaBH ₄	2240	[5]
Co-B-F	NaBH ₄	3400	[6]
Ni-Co-B hollow nanospheres	NaBH ₄	6400	[7]
Hollow Ni-Fe-B nanochain	NaBH ₄	4320	[8]
(RuCo) ₁₀₀ C ₃₅₀	NaBH ₄	9310	[9]
LiCoO ₂	NaBH ₄	2090	[10]
Co-Mo-B	NaBH ₄	1281	[11]
Co-B-P	NaBH ₄	3976	[12]
NiB/NiFe ₂ O ₄	NaBH ₄	300	[13]
Nickel-based complex	NaBH ₄	2240	[14]
NiCo ₂ O ₄ hollow sphere	NaBH ₄	1000	[15]
Porous Co ₂ P nanowire	NaBH ₄	4028	[16]
CoB/Ni-foam	NaBH ₄	1930	[17]
Ru/PPy	NaBH ₄	22740	[18]
Co incorporated magnetite-multiwalled carbon nanotube nanocomposites	NaBH ₄	1213	[19]
Catkin-like CoB	NaBH ₄	3120	[20]
Co-B/Cu sheet	NaBH ₄	7936	[21]
Co-Ni complex catalyst	NaBH ₄	330	[22]
Mesoporous silica nanospheresupported Pt nanoparticles	NaBH ₄	19000	[23]
FeCo ₂ O ₄ nanowire array	NaBH ₄	2551	[24]

supported on carbon cloth			
Ru nanoparticles supported on xonotlite nanowire	NaBH ₄	624	[25]
Co-W-P alloy	NaBH ₄	11820	[26]
Mo-modified Co-B	NaBH ₄	4200	[27]
Co-B-TiO ₂ framework	NaBH ₄	1980	[28]
Au/Co	NaBH ₄	2070	[29]
Pt/Co	NaBH ₄	4880	[30]
Pd/Co	NaBH ₄	9530	[31]
Pt/Ni	NaBH ₄	14800	[32]
Au/Ni	NaBH ₄	2340	[33]

Table S2 Comparison of apparent activation energy (E_a) values of Co-based catalysts from the literature.

Catalyst	Reactant	activation energy (kJ/mol)	Reference
Co	KBH ₄	44.2	Present work
Pt/Co	NaBH ₄	61.8	[30]
Pd/Co	NaBH ₄	54.0	[31]
CuCoNi	NaBH ₄	40.6	[34]
Raney Co	NaBH ₄	53.7	[35]
Co-P	NaBH ₄	60.2	[36]
Co-B	NaBH ₄	64.9	[37]
Ni-Co-B	NaBH ₄	62.0	[38]
Intrazeolite Co(0)	NaBH ₄	57.0	[39]
Co-Cu-B	NaBH ₄	49.6	[40]
Co-Mn-B	NaBH ₄	52.1	[41]
Co/SiO ₂	NaBH ₄	59.0	[42]

Table S3 Calculated binding energies of Co single atom and Co₄ cluster on stabilizing agent.

Co single atom	Binding energies (kJ/mol)	Co ₄ cluster	Binding energies (kJ/mol)
PVA-Co	-42.3	PVA-Co ₄	-62.5
PEG-Co	-52.6	PEG-Co ₄	-72.7
PVP-Co	-91.1	PVP-Co ₄	-113.1
Starch-Co	-91.9	Starch-Co ₄	-108.2
CMC-Na-Co	-42.4	CMC-Na-Co ₄	-91.0
PAAS-Co	-39.1	PAAS-Co ₄	-90.1
ISOBAM-Co_COO ⁻	-191.7	ISOBAM-Co ₄ _COO ⁻	-232.1
ISOBAM-Co_CONH ₂	-180.6	ISOBAM-Co ₄ _CONH ₂	-198.2
ISOBAM-Co_OCOCO	-173.5	ISOBAM-Co ₄ _OCOCO	-188.4

Table S4 Calculated activation energy (E_a) and reaction energy (E_r) of the first elementary step in the borohydride hydrolysis catalyzed by Co₄-ISO, Pt₄-ISO, Pd₄-ISO or Rh₄-ISO.

	E_a (kJ/mol)	E_r (kJ/mol)
Co ₄ -ISO	31.0	-33.5
Pt ₄ -ISO	72.0	24.3
Pd ₄ -ISO	80.3	28.9
Rh ₄ -ISO	46.4	-2.5

References

- 1 Lu, L., Zhang, H., Zhang, S. & Li, F. A Family of High-Efficiency Hydrogen-Generation Catalysts Based on Ammonium Species. *Angew. Chem. Int. Ed.* 54, 9328-9332 (2015).
- 2 Wei, Y. *et al.* Highly efficient and reactivated electrocatalyst of ruthenium electrodeposited on nickel foam for hydrogen evolution from NaBH₄ alkaline solution. *Int. J. Hydrogen Energy* 43, 592-600 (2018).
- 3 Wei, L. *et al.* Co₃O₄ hollow fiber: An efficient catalyst precursor for hydrolysis of sodium borohydride to generate hydrogen. *Int. J. Hydrogen Energy* 43, 1529-1533 (2018).
- 4 Kilinc, D., Sahin, O. & Saka, C. Salicylaldehyde-Ni complex supported on Al₂O₃: Highly efficient catalyst for hydrogen production from hydrolysis of sodium borohydride. *Int. J. Hydrogen Energy* 43, 251-261 (2018).
- 5 Kilinc, D. & Sahin, O. Synthesis of polymer supported Ni (II)-Schiff Base complex and its usage as a catalyst in sodium borohydride hydrolysis. *Int. J. Hydrogen Energy* 43, 10717-10727 (2018).
- 6 Izgi, M. S., Sahin, O., Odemis, O. & Saka, C. Microwave treatment and fluorine addition on Co-B catalyst to improve the hydrogen production rate. *Mater. Manuf. Process.* 33, 196-201 (2018).
- 7 Guo, J., Hou, Y., Li, B. & Liu, Y. Novel Ni-Co-B hollow nanospheres promote hydrogen

- generation from the hydrolysis of sodium borohydride. *Int. J. Hydrogen Energy* 43, 15245-15254 (2018).
- 8 Guo, J., Hou, Y. & Li, B. Facile synthesis of a hollow Ni-Fe-B nanochain and its enhanced catalytic activity for hydrogen generation from NaBH₄ hydrolysis. *Rsc Adv.* 8, 25873-25880 (2018).
 - 9 Arzac, G. M. *et al.* Strong activation effect on a Ru-Co-C thin film catalyst for the hydrolysis of sodium borohydride. *Sci. Rep.* 8, 9755 (2018).
 - 10 Wilcox, M. J. & Groven, L. J. Solution combustion synthesized lithium cobalt oxide as a catalytic precursor for the hydrolysis of sodium borohydride. *Int. J. Hydrogen Energy* 42, 6765-6770 (2017).
 - 11 Wei, Y. *et al.* Hydrogen generation from alkaline NaBH₄ solution using a dandelion-like Co-Mo-B catalyst supported on carbon cloth. *Int. J. Hydrogen Energy* 42, 9945-9951 (2017).
 - 12 Sahin, O., Karakas, D. E., Kaya, M. & Saka, C. The effects of plasma treatment on electrochemical activity of Co-B-P catalyst for hydrogen production by hydrolysis of NaBH₄. *J. Energy Inst.* 90, 466-475 (2017).
 - 13 Liang, Z., Li, Q., Li, F., Zhao, S. & Xia, X. Hydrogen generation from hydrolysis of NaBH₄ based on high stable NiB/NiFe₂O₄ catalyst. *Int. J. Hydrogen Energy* 42, 3971-3980 (2017).
 - 14 Kilinc, D., Sahin, O. & Saka, C. Investigation on salicylaldehyde-Ni complex catalyst as an alternative to increasing the performance of catalytic hydrolysis of sodium borohydride. *Int. J. Hydrogen Energy* 42, 20625-20637 (2017).
 - 15 Jadhav, A. R., Bandal, H. A. & Kim, H. NiCo₂O₄ hollow sphere as an efficient catalyst for hydrogen generation by NaBH₄ hydrolysis. *Mater. Lett.* 198, 50-53 (2017).
 - 16 Huang, X., Wu, D. & Cheng, D. Porous Co₂P nanowires as high efficient bifunctional catalysts for 4-nitrophenol reduction and sodium borohydride hydrolysis. *J. Colloid Interf. Sci.* 507, 429-436 (2017).
 - 17 Guo, S. *et al.* Highly stable and controllable CoB/Ni-foam catalysts for hydrogen generation from alkaline NaBH₄ solution. *Int. J. Hydrogen Energy* 42, 21063-21072 (2017).
 - 18 Baydaroglu, F. O., Ozdemir, E. & Gurek, A. G. Ruthenium nanoparticles immobilized on surfactant-directed polypyrrole as an effective and reusable catalyst for hydrogen generation. *React. Kinet. Mech. Cat.* 122, 575-591 (2017).
 - 19 Bandal, H. A., Jadhav, A. R. & Kim, H. Cobalt impregnated magnetite-multiwalled carbon nanotube nanocomposite as magnetically separable efficient catalyst for hydrogen generation by NaBH₄ hydrolysis. *J. Alloy. Compd.* 699, 1057-1067 (2017).
 - 20 Yan, J. J. *et al.* Capping-agent-free Synthesis of Catkin-like CoB Microstructures Composed of Ultrathin Nanosheets and Their Catalytic Performance in the Hydrolysis of Sodium Borohydride. *Int. J. Electrochem. Sc.* 11, 226-232 (2016).
 - 21 Wang, Y. *et al.* Catalytic hydrolysis of sodium borohydride via nanostructured cobalt-boron catalysts. *Int. J. Hydrogen Energy* 41, 276-284 (2016).
 - 22 Sahin, O., Kilinc, D. & Saka, C. Bimetallic Co-Ni based complex catalyst for hydrogen production by catalytic hydrolysis of sodium borohydride with an alternative approach. *J. Energy Inst.* 89, 617-626 (2016).
 - 23 Irum, M., Zaheer, M., Friedrich, M. & Kempe, R. Mesoporous silica nanosphere supported platinum nanoparticles (Pt@MSN): one-pot synthesis and catalytic hydrogen generation. *Rsc Adv.* 6, 10438-10441 (2016).

- 24 Hao, S. *et al.* Self-supported spinel FeCo₂O₄ nanowire array: an efficient non-noble-metal catalyst for the hydrolysis of NaBH₄ toward on-demand hydrogen generation. *Nanotechnology* 27 (2016).
- 25 Akbayrak, S. & Ozkar, S. Inverse relation between the catalytic activity and catalyst concentration for the ruthenium(0) nanoparticles supported on xonotlite nanowire in hydrogen generation from the hydrolysis of sodium borohydride. *J. Mol. Catal. A-Chem.* 424, 254-260 (2016).
- 26 Wang, L., Li, Z., Liu, X., Zhang, P. & Xie, G. Hydrogen generation from alkaline NaBH₄ solution using electroless-deposited Co-W-P supported on gamma-Al₂O₃. *Int. J. Hydrogen Energy* 40, 7965-7973 (2015).
- 27 Ke, D. *et al.* Kinetics study on hydrolytic dehydrogenation of alkaline sodium borohydride catalyzed by Mo-modified Co-B nanoparticles. *Int. J. Hydrogen Energy* 40, 7308-7317 (2015).
- 28 Cheng, J. *et al.* Highly active nanoporous Co-B-TiO₂ framework for hydrolysis of NaBH₄. *Ceram. Int.* 41, 899-905 (2015).
- 29 Wang, X. *et al.* Preparation and Catalytic Activities of Au/Co Bimetallic Nanoparticles for Hydrogen Generation from NaBH₄ Solution. *J. Nanosci. Nanotechnol.* 15, 2770-2776 (2015).
- 30 Cheng, J. *et al.* Preparation of Colloidal Pt/Co Bimetallic Nanoparticle Catalysts and Their Catalytic Activity for Hydrogen Generation from Hydrolysis Reaction of NaBH₄. *Rare Metal Mat. Eng.* 43, 2209-2214 (2014).
- 31 Zhao, W. G. *et al.* Preparation of Pd/Co Bimetallic Nanoparticles and Their Catalytic Activity for Hydrogen Generation. *Acta Phys.-Chim. Sin.* 31, 145-152 (2015).
- 32 Kong, D. C. *et al.* Preparation of Colloidal Pt /Ni Bimetallic Nanosols and Their Catalytic Activities for Hydrogen Generation from Hydrolysis Reaction of Sodium Borohydride. *Chem. J. Chin. Univ.* 34, 2377-2382 (2013).
- 33 Wang, X., Sun, S., Huang, Z., Zhang, H. & Zhang, S. Preparation and catalytic activity of PVP-protected Au/Ni bimetallic nanoparticles for hydrogen generation from hydrolysis of basic NaBH₄ solution. *Int. J. Hydrogen Energy* 39, 905-916 (2014).
- 34 Wang, X. *et al.* In situ synthesis of cobalt-based tri-metallic nanosheets as highly efficient catalysts for sodium borohydride hydrolysis. *Int. J. Hydrogen Energy* 41, 219-226 (2016).
- 35 Liu, B. H., Li, Z. P. & Suda, S. Nickel- and cobalt-based catalysts for hydrogen generation by hydrolysis of borohydride. *J. Alloy. Compd.* 415, 288-293 (2006).
- 36 Zhang, X. *et al.* Electroless-deposited Co-P catalysts for hydrogen generation from alkaline NaBH₄ solution. *Int. J. Hydrogen Energy* 35, 8363-8369 (2010).
- 37 Jeong, S. U. *et al.* A study on hydrogen generation from NaBH₄ solution using the high-performance Co-B catalyst. *J. Power Sources* 144, 129-134 (2005).
- 38 Ingersoll, J. C., Mani, N., Thenmozhiyal, J. C. & Muthaiah, A. Catalytic hydrolysis of sodium borohydride by a novel nickel-cobalt-boride catalyst. *J. Power Sources* 173, 450-457 (2007).
- 39 Rakap, M. & Ozkar, S. Intrazeolite cobalt(0) nanoclusters as low-cost and reusable catalyst for hydrogen generation from the hydrolysis of sodium borohydride. *Appl. Catal. B-Environ.* 91, 21-29 (2009).
- 40 Ding, X. L., Yuan, X. X., Jia, C. & Ma, Z. F. Hydrogen generation from catalytic hydrolysis of sodium borohydride solution using Cobalt-Copper-Boride (Co-Cu-B) catalysts. *Int. J.*

Hydrogen Energy 35, 11077-11084 (2010).

- 41 Yuan, X., Jia, C., Ding, X.-L. & Ma, Z.-F. Effects of heat-treatment temperature on properties of Cobalt-Manganese-Boride as efficient catalyst toward hydrolysis of alkaline sodium borohydride solution. *Int. J. Hydrogen Energy* 37, 995-1001 (2012).
- 42 Shih, Y.-J., Su, C.-C., Huang, Y.-H. & Lu, M.-C. SiO₂-supported ferromagnetic catalysts for hydrogen generation from alkaline NaBH₄ (sodium borohydride) solution. *Energy* 54, 263-270 (2013).